Spring 1979

Coupling Efficiency and Alignment Sensitivity of Single Mode Optical Fibers

James Mathew Martin
University of Central Florida

COUPLING EFFICIENCY AND ALIGNMENT SENSITIVITY OF SINGLE MODE OPTICAL FIBERS

BY

JAMES MATHEW MARTIN
B.S., Springhill College, 1969
M.S., Rollins College, 1973

THESIS

Submitted in partial fulfillment of the requirements
for the degree of Master of Science
in the Graduate Studies Program of the College of Engineering
of the University of Central Florida At Orlando, Florida

Spring Quarter
1979

COUPLING EFFICIENCY AND ALIGNMENT SENSITIVITY OF SINGLE MODE OPTICAL FIBERS

BY

JAMES MATHEW MARTIN

ABSTRACT

Coupling efficiency and alignment sensitivity models for the coupling of light from a fundamental mode Gaussian light beam into a single mode optical fiber are given. Experimental results are presented which verify the coupling and misalignment predictions of the models. Data were taken at two wavelengths: 0.6328 and 0.8460 micrometers. The light sources were a HeNe laser and a GaAlAs laser respectively. Coupling efficiencies were measured versus beam spot size; and lateral, axial and angular misalignments of the beam and fiber axes.

Sedki M. Riad

Dr. Sedki Riad

ACKNOWLEDGMENT

The modeling and experimental work were performed under contract DASG60-75-C-0060 Advanced Electronics and Digital Sensors Technology. The sponsoring agency is the Ballistic Missile Defense Advanced Technology Center Huntsville, Alabama. The contract monitor is Mr. Buster E. Kelley. Preparation of the thesis paper was performed under the direction of the Graduate Studies Program of the College of Engineering of the University of Central Florida at Orlando, Florida. Support for the presentation of this thesis paper was provided by the Martin Marrietta Corporation. The writing of this thesis paper was done on the author's time.

Assistance in the work by Dr. William Brockett, Mr. Jon Hoimes and Miss Connie Gill is gratefully acknowledged. Dr. Brockett set up the gallium aluminum arsenide laser, Mr. Hoimes and Miss Gill prepared optical fiber cables used in the experiments and Miss Gill and Mr. Hoimes assisted in taking parts of the data on fiber coupling.

The assistance and patience of my family who endured the many hours of writing is lovingly acknowledged.

The direction and assistance of Dr. Sedki Riad of the University of Central Florida who was the thesis advisor is also greatfully acknoledged.

PREFACE

The purpose of this thesis work is the experimental verification of coupling efficiency and alignment sensitivity models for single mode optical fibers. Prior to this work, no systematic data on coupling performance of single mode fibers had been presented. Typically, a publication on coupling modeling presents a single data point without details of the test conditions or repeatibility of the measurement. The work presented here verifies the coupling models with detailed coupling test results on two single mode optical fibers which had different cut-off wavelengths. The fiber designs were the same in all other respects. One fiber was designed to be a single mode fiber at the helium neon laser wavelength of 0.6328 micrometers and the other fiber was designed to be a single mode fiber at the gallium aluminum arsenide laser wavelength of 0.8500 micrometers. The fiber's coupling efficiency was measured versus lateral, axial (focal shift), and angular misalignment of the fiber with respect to the axis of the input light beam. The results of the experimental measurements are in good agreement with the coupling and misalignment effect predictions of the coupling model.

In Chapter I, beginning with waveguide mode expressions given

in Snyder (1969a), a model for the coupling of Gaussian beams into single mode optical fibers is developed. Misalignment models for lateral, axial, and angular misalignments are also developed. The misalignment models were included in the coupling efficiency model so that the effects of misalignments on coupling efficiency could also be predicted.

In Chapter II, the experimental set-ups used in this study are described. For each set-up, the test parameters are given. Techniques of data reduction used are described. Experimental results are presented in tables and graphs. The coupling efficiency and alignment effects predicted by the coupling model are shown with the data.

In Chapter III, the experimental results are discussed and compared to the corresponding model predictions. Also, conclusions on methods of minimizing misalignment sensitivity are presented.

CONTENTS

CHAPTER I

THEORY OF OPTICAL FIBER MODE EXCITATION

Light propagation in optical fibers is described by solutions to the wave equation with appropriate boundary conditions applied. The solutions obtained are a set of orthogonal eigenfunctions. Each eigenfunction describes a propagating mode in the optical fiber waveguide. The fundamental propagating mode is of particular importance since an optical fiber can be designed which propagates light only in the fundamental mode.

The fiber optic modes are excited by coupling light into one end of a fiber. It is desirable to know how large a fraction of light incident on a fiber end is coupled into the fiber and how accurately the fiber must be aligned for efficient coupling. Usually, a lens is used to focus the light beam onto the fiber end. A lens is needed since the fiber core is quite small. An optical beam which has a diameter equal to the fiber core diameter will expand rapidly as it propagates. Thus, a light beam of larger diameter than the core (typically 100 times larger) propagates to a coupling lens which focuses the beam down to the fiber's core diameter.

The coupling situation considered in this paper is that of a coupling beam propagating to the fiber end through an unbounded medium (no waveguide structure). In an unbounded medium, a continuum of modes exists. Of these modes those of most interest are the Gaussian beam modes. The Gaussian beam modes are important because they describe the distribution and propagation characteristics of light from lasers. The Gaussian beam modes occur in the Fabry-Perot interferometer. Lasers incorporate a Fabry-Perot interferometer to form their resonant cavity. Thus, laser light propagation properities are described by the Gaussian beam modes. Therefore, the coupling of laser light into an optical fiber end can be modeled as the excitation of optical fiber waveguide modes by incident light propagating in Gaussian beam modes. For single mode fibers, the efficiency of coupling light into the fundamental waveguide mode is of interest. The fundamental Gaussian beam mode best matches the optical fiber's fundamental waveguide mode. Further, lasers can be designed to produce a fundamental Gaussian beam output without higher order modes present. Thus, high coupling efficiency of the laser output power into a single mode fiber can be obtained.

In this Chapter a model for optical fiber waveguide mode excitation by the fundamental Gaussian beam mode is presented. The model is based upon simplified approximate waveguide mode expressions developed by Snyder(1969a). Coupling efficiency expressions are developed by the methods used in Snyder(1969b). The coupling of light in

Gaussian beam modes is developed similar to the work by Stern(1970). Modeling of misalignment effects follows the work of Stern(1971) and Marcuse(1970) for lateral misalinment and the work of Imai(1973) for angular misalignment. The model development consists of four parts. The first part reviews the mode equations for Gaussian beams. The second part presents the equations of the modes in an optical fiber. The development of the expressions for the modes is outlined in the Appendix. The third part presents the development of the coupling equation. The fourth part presents the modeling of the sensitivity of coupling to misalignments.

Gaussian Beam Modes

The Gaussian beam modes are designated $TEM_{m,n}$ for transverse electric and magnetic fields. m and n specify the mode. The characteristics of Gaussian beams have been derived by a number of authors. Yariv (1971) and Marcuse (1972) present detailed discussions. A synopsis of the derivation is given here.

The most direct approach to the derivation begins with the scalar wave equation and the approximation of paraxial rays and the assumption of slowly varying fields along the z axis. Using these assumptions and the further restriction of an isotropic medium, the following scalar wave equation is obtained (Yariv 1971).

$$\nabla_t^2\psi - 2ik\partial\psi/\partial z = 0 \qquad \text{(I-1)}$$

Where ψ is a scalar field usually taken to be proportional to the electric field by the relation

$$E = \psi(x,y,z)\exp(-ikz) \qquad \text{(I-2)}$$

k is the propagation constant equal to $2\pi/\lambda$, where λ is the wavelength of the light beam. ∇_t^2 is the transverse part of the Laplace operator.

The fundamental mode solution to (I-1) is of the form

$$E(x,y,z) = E_0\frac{\omega_0}{\omega(z)}\exp\left[-i(kz - \phi) - r^2\left(\frac{1}{\omega^2(z)} + \frac{ik}{2R}\right)\right] \qquad \text{(I-3)}$$

Where E_0 is the electric field amplitude on the z axis. $\omega(z)$ is the beam radius at which the amplitude has fallen to 1/e of its on axis value. ω_0 is the smallest beam radius defined at z = 0. R is the radius of curvature of the beam phase front. ϕ is a beam phase term. The following relationships relate ω, R and ϕ to ω_0, z and λ.

$$\omega(z)^2 = \omega_0^2 \left[1 + \left(\frac{\lambda z}{\pi \omega_0^2} \right)^2 \right] \tag{I-4}$$

$$R(z) = z \left[1 + \left(\frac{\pi \omega_0^2}{\lambda z} \right)^2 \right] \tag{I-5}$$

$$\phi(z) = \tan^{-1} \left(\frac{\lambda z}{\pi \omega_0^2} \right) \tag{I-6}$$

The above expressions show that once the initial beam waist at $z = 0$ is known, the subsequent propagation characteristics of the beam are determined. Figure 1 illustrates the parameters of the Gaussian beam and the behavior of a Gaussian beam near a lens' focal plane.

The field distribution described by (I-3) is called the fundamental Gaussian beam mode. Note that perpendicular to the axis it has a Gaussian distribution. This beam mode is one of a set of modes described by a more general solution to (I-1). The more general field expression for the $TEM_{m,n}$ mode is

$$E_{m,n}(x,y,z) = E_0 \frac{\omega_0}{\omega} H_m(\sqrt{2}x/\omega) H_n(\sqrt{2}y/\omega) \exp \left[-r^2 \left(\frac{1}{\omega_0^2} + \frac{ik}{2R} \right) - ikz + i(m + n + 1)\phi \right] \tag{I-7}$$

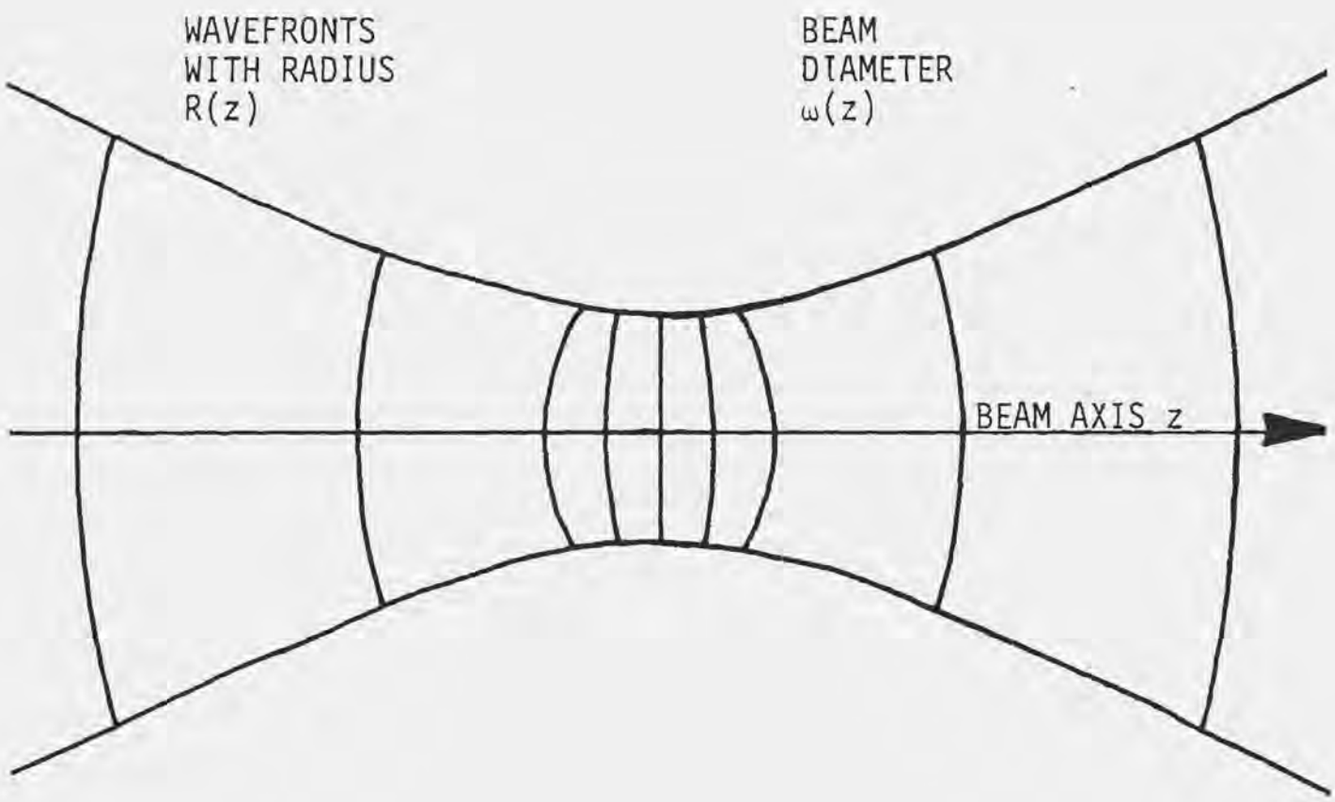

Figure 1. Propagation characteristics of a Gaussian beam.

Where H_m and H_n are Hermite polynomials of order m and n. When m=n=o H_o = 1 which when substituted into (I-7) yields the fundamental Gaussian beam.

An additional result needed in the analysis of fiber optic coupling is normalization of the Gaussian beam expression (I-3). Since the power coupling efficiency will be the end result, the Gaussian beam normalization must be in terms of beam power. The power density in an optical beam is given by the Poynting vector $\vec{S}$, given by

$$\vec{S} = \vec{E} \times \vec{H}^* \qquad \text{(I-8)}$$

Where $\vec{H}$ is the magnetic field strength.
In isotropic media $\vec{E}$ and $\vec{H}$ are related as follows:

$$\vec{H} = \sqrt{\frac{\varepsilon_1}{\mu}}\, \hat{z} \times \vec{E} \qquad \text{(I-9)}$$

Where μ is the medium premeability, ε_1 is its dielectric constant and $\hat{z}$ is a unit vector in the direction of beam propagation. Substitution of (I-9) into (I-8) and using the triple vector product identity yields

$$\vec{S} = \sqrt{\varepsilon_1/\mu}\, E^2 \hat{z} \qquad \text{(I-10)}$$

The power contained in the beam is obtained by integration of the time averaged Poynting vector over the beam cross section. The time dependence of $\vec{S}$, given by (I-10), is that of $\vec{E}$. $\vec{E}$ has a harmonic time dependence of the form

$$\vec{E}(x,y,z,t) = \vec{E}(x,y,z)\cos(2\pi ft) \qquad \text{(I-11)}$$

Where f is the optical frequency. Substitution of (I-11) into (I-10) yields

$$\vec{S} = \sqrt{\varepsilon_1/\mu}\, E(x,y,z)^2 \cos^2(2\pi ft)\hat{z} \qquad \text{(I-12)}$$

Integration of (I-12) over one period of oscillation yields

$$\langle \vec{S} \rangle = \frac{1}{2} \sqrt{\varepsilon_1/\mu}\, E(x,y,z)^2 \hat{z} \tag{I-13}$$

Integration of (I-13) over the beam cross section in polar coordinates yields

$$P = \frac{1}{2}\sqrt{\varepsilon_1/\mu}\left(E_0 \frac{\omega_0}{\omega}\right)^2 \int_0^{\infty}\int_0^{2\pi} \exp(-2r^2/\omega^2) r\,dr\,d\psi$$

$$P = \pi\sqrt{\varepsilon_1/\mu}(E_0\omega_0/2)^2 \tag{I-14}$$

An expression for E_0, the normalized electric field, is obtained when P is set equal to unity. The expression is

$$E_0 = \left[\frac{4\sqrt{\mu/\varepsilon_1}}{\pi\omega_0^2}\right]^{1/2} \tag{I-15}$$

Substitution of (I-15) into (I-3) yields the power normalized Gaussian beam field expression.

$$E(x,y,z) = \left[\frac{4\sqrt{\mu}/\varepsilon_1}{\pi\omega^2}\right]^{-1/2} \exp\left[-i(kz - \phi) - r^2\left(\frac{1}{\omega^2} + \frac{ik}{2R}\right)\right] \qquad \text{(I-16)}$$

This expression is used later in the derivation of the expression for coupling efficiency of a Gaussian fundamental mode beam into an optical fiber fundamental mode.

Optical Fiber Modes

The guided wave field expressions for optical fibers are the same as the expressions that describe the guiding of millimeter waves. Solutions to the wave equation in cylindrical coordinates in dielectric media describe the transport of light in fiber optics (Marcuse 1972). Even for the lowest order mode, the hybrid HE_{11} mode, the exact field expressions and boundary conditions are quite complex. Snyder (1969a) has derived accurate, simpler approximations of the expressions describing fiber optic modes and their boundary conditions. Experiments described in Chapter II are compared to predictions based upon the expressions developed by Snyder and good agreement is shown.

Figure 2 illustrates the model used to analyze the modes of optical fiber waveguides. The radial coordinate is ρ. In the analysis a normalized radial coordinate r is defined in units of the fiber optic core radius, a. Thus, r is given by $r = \rho/a$.

Snyder assumed asymptotic solutions to the wave equation for a cylindrical boundary on a dielectric rod of dielectric constant ε_1 and a semi-infinite surrounding medium of dielectric constant ε_2. The condition for the asymptotic solution to be valid is that $ak \gg 1$. Where a is the rod radius and k is the plane wave propagation constant in the medium. The eigenvalue and eigenfunction equation are expanded in power series of the quantity u_p/ak. u_p is the pth mode eigenvalue for the normalized modal propagation constant, β, in the dielectric rod. u_p is given by

$$u_p^2 = (ak_1c)^2\mu - \beta_p^2 , \quad r \leq 1 \tag{I-17}$$

Where k_1 is the plane wave propagation constant in medium of dielectric constant ε_1 and is given by

$$k_1 = 2\pi n_1/\lambda \tag{I-18}$$

c is the speed of light in vacuum and μ is the permeability of the medium. Outside the dielectric rod the propagation is defined by the eigenvalue w_p given by

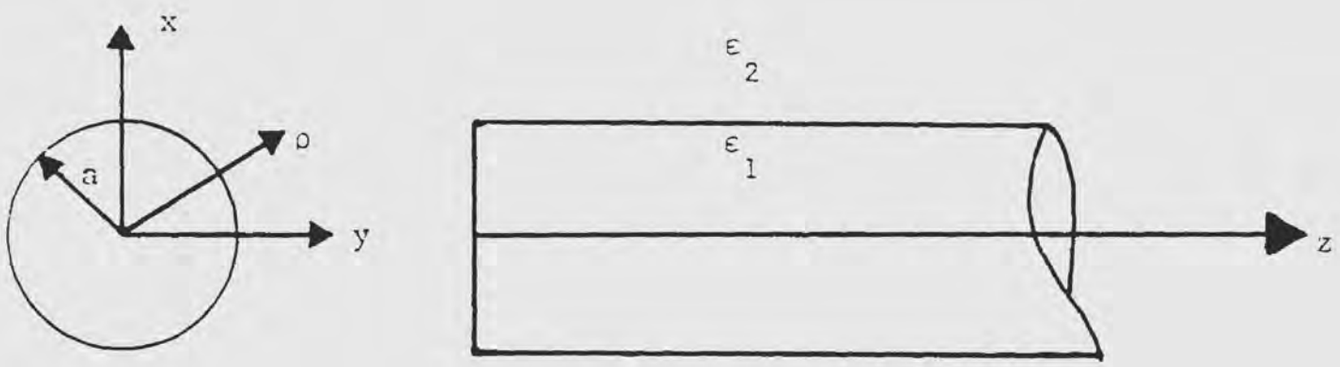

Figure 2. Fiber optic model: Rod of dielectric constant ε_1 in a semi-infinite medium of dielectric constant ε_2.

$$w_p = \beta_p^2 - (ak_2c)^2, \; r \geq 1 \qquad \text{(I-19)}$$

Where k_2 is the plane wave propagation constant in the medium of dielectric constant ε_2 and is given by

$$k_2 = 2\pi n_2/\lambda \qquad \text{(I-20)}$$

Snyder also uses the assumption that $1-(\varepsilon_1/\varepsilon_2)<<1$ which is valid for single mode optical fibers for which the value is of the order of 0.002. This assumption allows expression of the magnetic field in the guide in terms of the electric field in the guide. Thus, only the electric field expression is needed in computations on the guide modes; greatly simplifying the computations.

The following expressions are those obtained by Snyder for the normalized transverse modal fields, $\vec{e}_p$. Since these expressions are normalized, they are directly usable in obtaining the coupling coefficients. Note that the expressions have been transformed to rectangular coordinates.

$$\vec{e}_p = \left[\hat{x}\begin{pmatrix} \sin(\ell \mp 1)\phi \\ \cos(\ell \mp 1)\phi \end{pmatrix} + \hat{y}\begin{pmatrix} \cos(\ell \mp 1)\phi \\ -\sin(\ell \mp 1)\phi \end{pmatrix} \right]$$

$$\cdot \begin{pmatrix} J_{\ell \mp 1}(Ur)/J_{\ell \mp 1}(U) & r \lessgtr 1 \\ K_{\ell \mp 1}(Wr)/K_{\ell \mp 1}(W) & r \gtrless 1 \end{pmatrix} (\psi_p)^{-1/2}$$

and for the magnetic field

$$\vec{h}_p = \sqrt{\varepsilon_1/\mu}\, \hat{z} \times \vec{e}_p \text{ for all } r. \qquad \text{(I-21)}$$

The boundary condition obtained by Snyder is given by

$$UJ_\ell(U)/J_{\ell \mp 1}(U) = \mp WK_\ell(W)/K_{\ell \mp 1}(W) \qquad \text{(I-22)}$$

The power normalization, ψ_p, is given by

$$\psi_p = \sqrt{\mu/\varepsilon_1}\ \pi a^2 (V/U)^2 K_\ell(W) \cdot$$
$$K_{\ell \mp 2}(W)/K_{\ell \mp 1}(W) \qquad \text{(I-23)}$$

Where V is the normalized frequency defined by the expression

$$V^2 = (ak_1c)^2 \mu\delta = U^2 + W^2 \qquad \text{(I-24)}$$

k_1 is the plane wave propagation constant in the rod medium and δ is defined by

$$\delta = 1 - (\varepsilon_1/\varepsilon_2) \qquad \text{(I-25)}$$

or using the relationship between dielectric constant and refractive index

$$\delta = 1 - (n_1/n_2)^2 \qquad \text{(I-26)}$$

U and W are first order approximations to the eigenvalues u_p and w_p respectively. In (I-21) the upper sign on the x component of

$\vec{e}_p$ applies for the HE_{1m} hybrid modes and the lower sign for the EH_{1m} hybrid modes. Also in (I-21) The choice of two ϕ dependencies allow choice of either an even azimuthal dependence by choosing the upper line or an odd azimuth dependence by choosing the lower line. The choice is arbitrary and does not affect the results. J_1 is the Bessel function of order 1 and K_1 the modified Bessel function of order 1.

Mode cutoff in optical fibers occurs at specific values of the normalized frequency, V. The first few guide modes and the associated V number range are given below (Miller 1976).

$$V = 0 - 2.4048\text{: } (2)\ HE_{11}$$

$$V = 2.4048 - 3.8317\text{: } (2)\ HE_{11},\ (2)\ TE_{01},\ (2)\ HE_{21},\ (2)\ TM_{01}$$

The numbers in parentheses are the mode degeneracies.

The single mode fiber is designed with a value of V less than 2.405 so that only one mode, the HE_{11} lowest order hybrid mode, will propagate. The distribution of the transverse HE_{11} mode fields is obtained from (I-21) when the subscripts 1 and m are both equal to one. Using this value for 1 and m the HE_{11} mode transverse fields are given by

$$\vec{e}_p = \begin{bmatrix} \hat{x} \\ \hat{y} \end{bmatrix} \begin{bmatrix} J_0(Ur)/J_0(U) & r \leq 1 \\ K_0(Wr)/K_0(W) & r \geq 1 \end{bmatrix} \cdot$$

$$\left(\frac{\mu}{\varepsilon_1}\right)^{-1/4} \left[\pi a^2 (V/W)^2 \left(J_1(U)/J_0(U)\right)^2\right]^{-1/2}$$

$$\vec{h}_p = \sqrt{\varepsilon_1/\mu}\ \hat{z} \times \vec{e}_p \qquad \text{(I-27)}$$

The boundary condition from (I-22) is given by

$$UJ_1(U)/J_0(U) = WK_1(W)/K_0(W) \qquad \text{(I-28)}$$

The symmetry of the modified Bessel function and the boundary condition (I-22) were used to simplify the normalization. The symmetry property of the modified Bessel function is $K_\ell = K_{-\ell}$ (Olver 1967).

Excitation of Optical Fiber Modes by Gaussian Beams

The method of launching waves on a fiber optic waveguide is to focus a light beam onto the fiber end. The analysis approach used here assumes that the dielectric rod or core diameter, 2a, is large compared to the wavelength. This is a valid assumption since for single mode fibers the core diameter is 5 to 10 times larger than the wavelength of light. Thus, the fiber end is treated as a dielectric interface and the fields produced are assumed to be those produced by wave reflection at a plane dielectric boundary. That this assumption is reasonable is supported by experimental results described in Chapter II. There, the experimentally determined coupling properties of single mode fibers are shown to be in good agreement with predictions based upon the assumptions used.

The modes of the optical fiber waveguide are assumed to form a complete orthogonal set so that the incident light beam's transverse field distribution can be represented by an expansion over the fiber modes and the radiation modes (Snyder 1969b). Thus, the Gaussian beam's transverse field given by (I-16) can be expressed as a linear combination of modes given by (I-21).

$$\vec{E}(x,y,z) = \sum a_p \vec{e}_p(x,y,z)$$

$$\vec{H}(x,y,z) = \sum a_p \vec{h}_p(x,y,z) \qquad \text{(I-29)}$$

It remains to determine the coefficients a_p. This is done in the usual way using the orthogonality of the guide modes given by

$$\int\int \vec{e}_p \times \vec{h}_q^* \cdot \hat{z}\,da = \begin{cases} 0 & p \neq q \\ 1 & p = q \end{cases} \qquad \text{(I-30)}$$

(Collin 1960)

Taking the cross product between the first of equations (I-29) and h_p, integrating over the fiber end-face and using the othogonality condition (I-30) yields for a_p

$$a_p = \int\int \vec{E} \times \vec{h}_p^* \cdot \hat{z}\,da \qquad \text{(I-31)}$$

Using (I-27), (I-31) becomes

$$a_p = \sqrt{\varepsilon_1/\mu} \int\int \vec{E} \times \hat{z} \times \vec{e}_p^* \cdot \hat{z}\,da \qquad \text{(I-32)}$$

By the properties of the scalar triple product the integrand of (I-32) becomes

$$\vec{E} \times (\hat{z} \times \vec{e}_p^*) \cdot \hat{z} = -\vec{E} \cdot (\hat{z} \times \vec{e}_p^* \times \hat{z})$$

$$= \vec{E} \cdot (\hat{z} \times \hat{z} \times \vec{e}_p^*)$$

$$= \vec{E} \cdot \vec{e}_p^* \qquad \text{(I-33)}$$

Thus, using (I-33), (I-32) becomes

$$a_p = \sqrt{\varepsilon_1/\mu} \int\int \vec{E} \cdot \vec{e}_p^* da \qquad \text{(I-34)}$$

Assume that the incident light beam is a Gaussian beam linearly polarized along the x-axis. Then (I-34) becomes

$$a_p = \sqrt{\varepsilon_1/\mu} \int\int \hat{x}E \cdot \begin{bmatrix} \hat{x} \\ \hat{y} \end{bmatrix} e_p^* da$$

Applying the dot product rules,

$$a_p = \sqrt{\varepsilon_1/\mu} \int \int E e_p^* da \qquad \text{(I-35)}$$

Substitution of (I-16) and (I-27) into (I-35) yields for a_p

$$a_p = \frac{2}{\pi\omega a} \frac{WJ_0(U)}{VJ_1(U)} \int_0^{2\pi} \int_0^{\infty} \begin{bmatrix} J_0(Ur)/J_0(U) & r \leq 1 \\ K_0(Wr)/K_0(W) & r \geq 1 \end{bmatrix} \cdot$$

$$\exp\left[-(r^2/\gamma^2) - i(kz - \phi) - i(r^2k/2\gamma^2R)\right] r dr d\phi \qquad \text{(I-36)}$$

Where the substitution $\gamma = a/\omega$ has been made. The explicit dependence of ω on z and thus γ on z is not shown.

The power coupled into a waveguide is the measurable quantity, thus, an expression for the fraction of the power in the incident wave coupled into each waveguide mode is of interest. The coupled mode power is obtained from the time averaged Poynting vector, $\vec{S}$, given by (I-8) The time average is given by

$$\langle \vec{S} \rangle = \int_0^T \vec{E} \times \vec{H}^* dt \qquad \text{(I-37)}$$

Where T is the period of the wave oscillation. It is assumed that linear superposition holds so that the frequencies present in the wave incident on the optical fiber end can be separately analyzed. Thus, the time dependence of $\vec{E}$ and $\vec{H}$ in (I-37) can be explicitly written as

$$\vec{E}(x,y,z,t) = \vec{E}(x,y,z)\cos(2\pi ft)$$

$$\vec{H}(x,y,z,t) = \vec{H}(x,y,z)\cos(2\pi ft) \qquad \text{(I-38)}$$

Substitution into (I-37) yields

$$\langle\vec{S}\rangle = \vec{E} \times \vec{H}^{*} \int_{0}^{T} \cos^{2}(2\pi ft)dt \qquad \text{(I-39)}$$

Thus,

$$\langle\vec{S}\rangle = \frac{1}{2}\vec{E} \times \vec{H}^{*} \qquad \text{(I-40)}$$

The $\vec{E}$ and $\vec{H}$ refer now only to the time independent part of the fields. The power, P, in the wave is given by integration over the surface normal to the direction of propagation.

$$P = \int\int \langle \vec{S} \rangle \cdot \hat{z} da = \frac{1}{2}\int\int \vec{E} \times \vec{H}^* \cdot \hat{z} da \qquad (I-41)$$

The fields in (I-41) are expressed in terms of waveguide modes by (I-29) which when substituted into (I-41) gives

$$P = \frac{1}{2}\int\int (\sum a_p \vec{e}_p) \times (\sum a_q^* \vec{h}_q^*) \cdot \hat{z} da \qquad (I-42)$$

Mode orthogonality is used to reduce (I-42) as follows.

$$P = \frac{1}{2}\sum a_p a_q^* \int\int \vec{e}_p \times \vec{h}_q^* \cdot \hat{z} da$$

$$P = \frac{1}{2}\sum a_p a_p^* \qquad (I-43)$$

The last step follows since the waveguide fields are normalized according to (I-30). From (I-43) the fraction of power coupled into a waveguide mode by a given incident wave can be determined. In

Chapter II experiments are described which investigated the power coupled from a fundamental mode Gaussian beam into the fundamental waveguide mode. According to (I-43) and (I-36) the power fraction of an incident fundamental mode Gaussian beam coupled into the fundamental waveguide mode is given by

$$P = \frac{1}{2}\left[\frac{4}{\omega a}\frac{WJ_0(U)}{VJ_1(U)}\int_0^{\infty}\begin{pmatrix} J_0(Ur)/J_0(U) & r\leq 1 \\ K_0(Wr)/K_0(W) & r\geq 1 \end{pmatrix}\cdot \exp(-r^2/\gamma^2)rdr\right]^2 \qquad \text{(I-44)}$$

In (I-44) the fiber is assumed to be at the beam focus at which $z = 0$. The phase term of the Gaussian beam is zero at $z = 0$.

Effects of Misalignments

(I-44) is the basic model for fiber coupling. It is compared in Chapter II to experimental coupling results. (I-44) must be modified to predict alignment sensitivities of single mode fibers. The real part of the exponential argument must be modified to

include axis misalignment and the phase term must be modified to include angular tilt of the fiber or beam axis.

Lateral misalignment

The geometry for lateral displacement is shown in Figure 3 and the model parameters are shown in Figure 4. In the Figures, the Gaussian beam axis is displaced by the amount d parallel to the optical fiber. The integration is performed over the fiber cross-section with integration variables r and ψ. For given r and ψ the corresponding radial position from the Gaussian beam center is given by the law of cosines.

$$r'^2 = r^2 + d^2 - 2rd\cos\psi \qquad \text{(I-45)}$$

Tilt Misalignment

Tilt misalignment refers to the angle between the optical fiber axis and the input beam's axis. The geometry for tilt misalignment is shown in Figure 5. The tilt misalignment model parameters are shown in Figures 6 and 7. Imai and Hara (1973) developed a tilt misalignment model. The following is an adaptation of their model with the condition $n_1 \simeq n_2$. In their model, the phase mismatch between the tilted input Gaussian beam and the fiber optic waveguide modes is shown to reduce coupling. For small axis tilt angles,

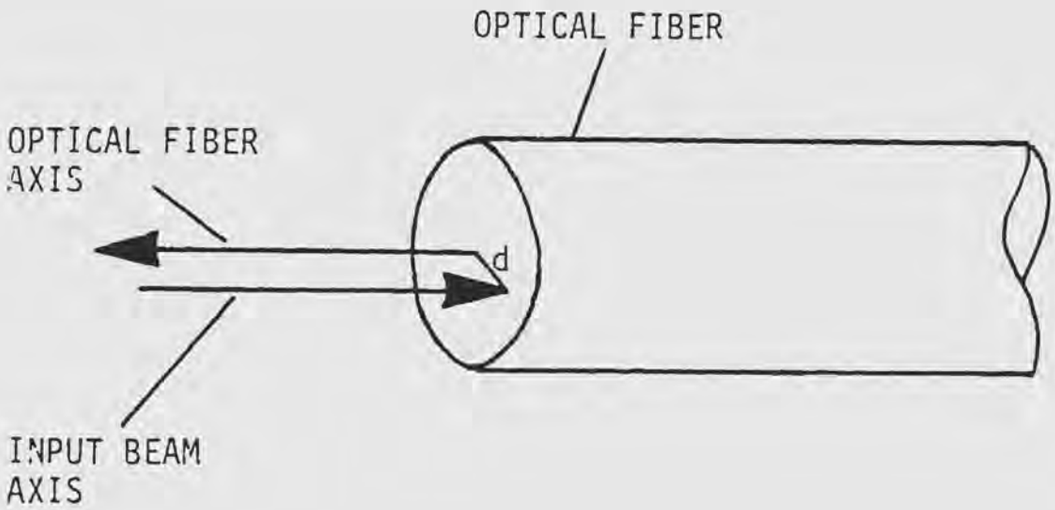

Figure 3. Lateral misalignment geometry. The distance d is the axis misalignment.

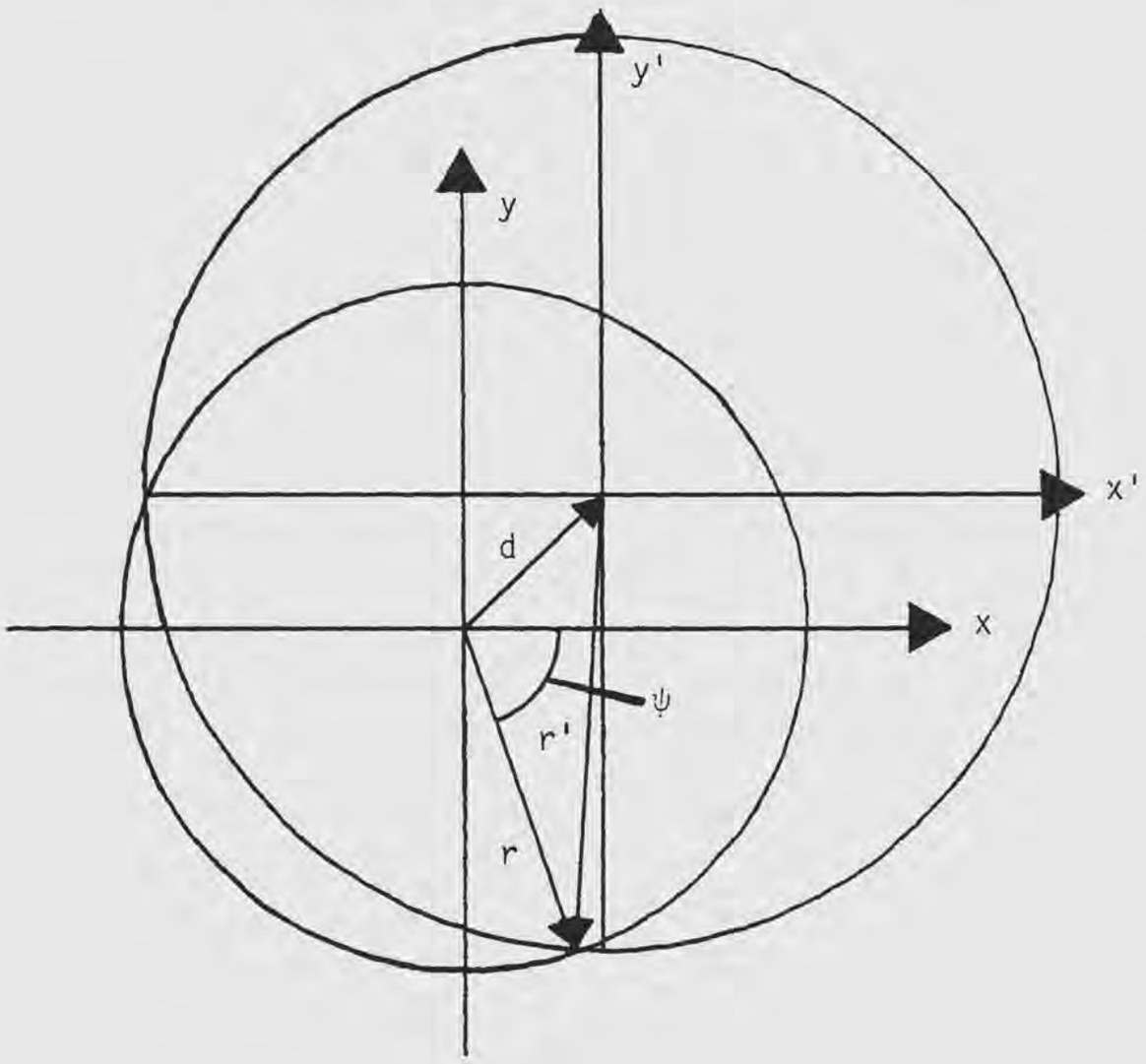

Figure 4. Lateral misalignment model.

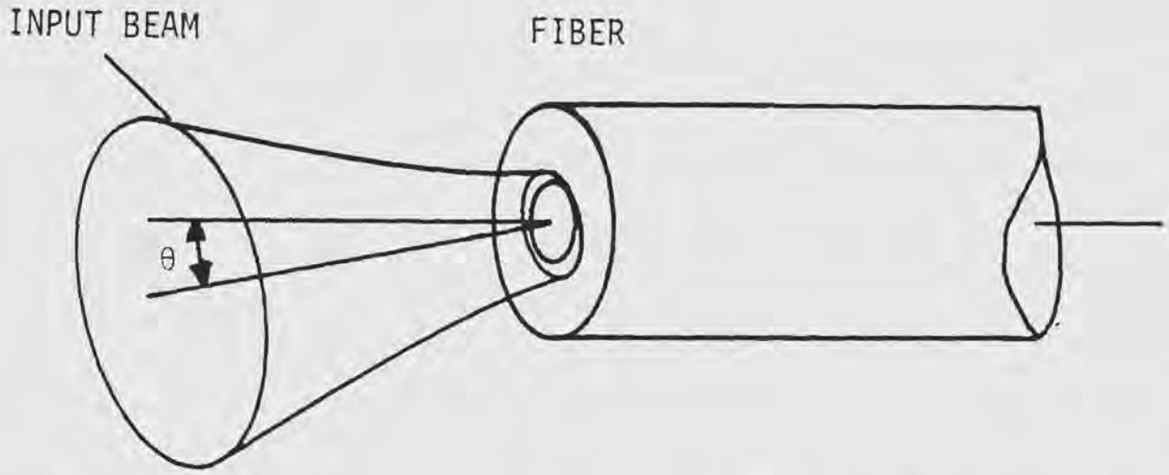

Figure 5. Tilt misalignment geometry. θ is the tilt angle of the beam axis with respect to the fiber axis.

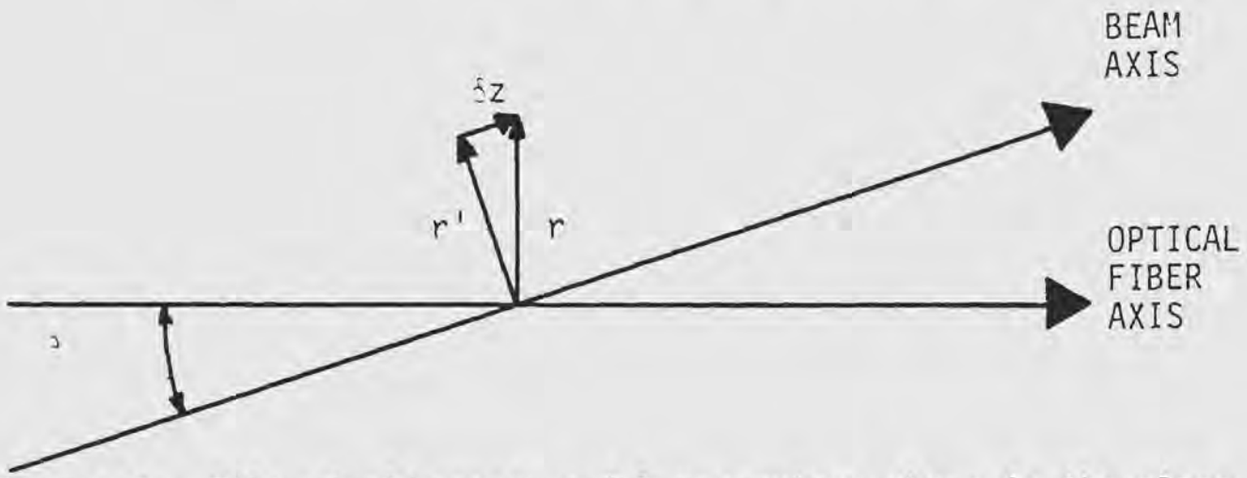

Figure 6. Tilt misalignment model parameters shown in the plane containing the tilt angle.

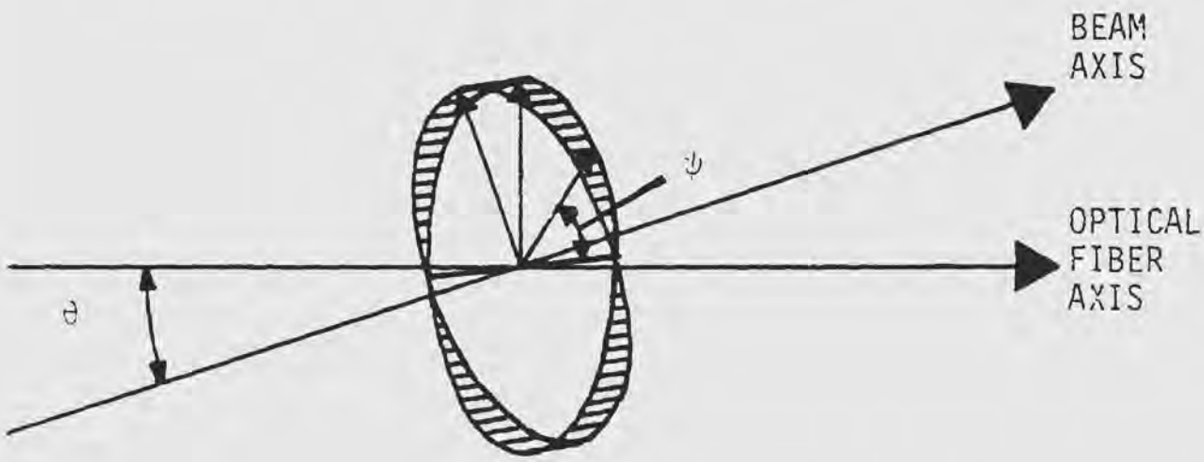

Figure 7. Variation of the axial displacement δz with the coordinate angle ψ.

the phase mismatch is the principle cause of coupling reduction. From (I-7) with the substitution of (I-6), the shape of the Gaussian beam phase front is given by

$$\alpha = k(z' + r'^2/2R) - \tan^{-1}(\lambda z'/\pi\omega_0^2) \qquad \text{(I-46)}$$

Where α is the phase of the beam at the position given by r' and z'. Circular symmetry of α about z is assumed. r' and z' are the coordinates of the input beam with respect to its axis and r and z are the coordinates associated with the fiber axis. The phase fronts of the waveguide modes are assumed planar. The phase mismatch is given by the relative phase between the input beam and the waveguide modes. Thus, the absolute value of z in (I-46) is not important. However, when the input beam axis is tilted with respect to the fiber's axis, the z-axis position on the beam axis becomes a function of the radial position with respect to the fiber axis. That is, when in the coupling expression the integral over the fiber face is performed, the beam cross-section contributing to the integral varies. The position on the input beam axis varies with fiber face coordinates according to the following expressions.

$$\delta z' = r\sin\theta\sin\psi$$

$$r' = r\cos\{\tan^{-1}(\tan\theta\sin\psi)\} \qquad \text{(I-47)}$$

These expressions come from the geometry shown in Figures 6 and 7.

The variation in z given by (I-47) also means that the phases of the input beam segments contributing to the integration are different. That is, the input beam phase on the fiber face is not constant over the face. To excite only the fundamental mode, the input beam must have constant phase over the fiber face. A curved phase front input beam will excite higher order modes. The single mode fiber won't propagate higher order modes, thus, their power radiates out of the fiber guide. Only the power in the fundamental mode propagates in the fiber. The radiated power is lost, thus, the coupling into the fiber is reduced.

The expressions for the phase front and z'-axis position can be simplified. The tilt angle at which the power coupling efficiency has reduced by 3dB is small. Thus, the small angle approximations can be used. Applying the small angle approximations (I-47) becomes

$$\delta z' \simeq r\theta\sin\psi$$

(I-48)

$$r' \simeq r$$

$\delta z'$ is small, thus, the spot size variation is negligible and the phase expression can be simplified. Most of the coupled power is contained within a radius less than a few core radii. Typical fiber core radii are less than 5 micrometers, thus, r is not greater than the order of 10 micrometers. Further, for tilt angle of 0.1 radians coupling is down 3 dB. Thus, θ is not greater than the order of 0.1 radian. Given these values for r and θ, $\delta z'$ is less than 1.0 micrometers.

The spot size dependence on z is given by (I-4)

$$\omega^2(z) = \omega_0^2 \left[1 + \left(\frac{\lambda z}{\pi \omega_0^2} \right)^2 \right] \qquad \text{(I-49)}$$

Typical values for λ and ω_0 are 0.5 micrometers and 5.0 micrometers respectively. By (I-49) the change in spot size is less than .004 per cent.

The phase expression, (I-46), can be simplified as follows. The change in the phase front radius of curvature, R, with $\delta z'$ is also negligible. The radius of curvature is given by

$$R(z) = z \left[1 + \left(\frac{\pi \omega_0^2}{\lambda z} \right)^2 \right] \qquad \text{(I-50)}$$

R has an asymptote at z = 0. For z near zero, the asymptotic expression for R is

$$R \simeq \left(\frac{\pi\omega_0^2}{\lambda}\right)^2 \frac{1}{z} \qquad \text{(I-51)}$$

Using the above values for ω_0 and λ, (I-51) with z replaced by z' takes the form

$$R = 25{,}000\ \mu m^2/z' \qquad \text{(I-52)}$$

Using (I-52), the second term of (I-46) for z near zero takes the form

$$kr^2/2R = 0.025\ \mu m^{-1} z' \qquad \text{(I-53)}$$

Where k was determined using the above value for λ and the previously determined value for r was used. It is now shown that $\delta z'$ affects (I-53) negligibly compared to the effect on the first term in (I-46), kz'. The value of k is $12.6 \mu m^{-1}$; thus, for $\delta z' = 1.0$ micrometers, the values for these phase terms are

$$kr^2/2R = 0.025 \text{ radians}$$

$$kz' = 12.6 \text{ radians}$$

Lastly, for z' near zero the small angle approximation for the tangent is used to approximate the third term of (I-46) by

$$\tan^{-1}(\lambda z'/\pi\omega_0^2) \simeq z'(\lambda/\pi\omega_0^2) \qquad \text{(I-54)}$$

Again using the above values for ω_0 and λ, (I-54) equals $0.0064\mu m^{-1}z'$. Compared to the other phase terms, this term is negligible.

It is assumed, therefore, that for tilt misalignments the coupling model does not need to include the changes in spot size and radius of curvature with $\delta z'$. Thus, the phase expression used in the model is the following.

$$\alpha = k(r\theta\sin\psi + r^2/2R) \qquad \text{(I-55)}$$

Where (I-48) has been substituted into (I-46) and the third term of (I-46) has been dropped. This expression for the beam phase was also used by Imai and Hara. The phase term kz is not needed in the model.

Focal Misalignment

Focal misalignment effects are included by utilizing the z dependence of the Gaussian beam parameters.

Misaligned Coupling

A power coupling expression including misalignment effects can

be obtained as follows. Substitution of (I-55) into (I-36) results in the following expression for a_0.

$$a_0 = \frac{2}{\pi\omega a}\frac{WJ_0(U)}{VJ_1(U)}\int_0^{2\pi}\int_0^{\infty}\begin{bmatrix} J_0(Ur)/J_0(U) & r\leq 1 \\ K_0(Wr)/K_0(W) & r\geq 1 \end{bmatrix}\cdot$$

$$\exp[\,-r'^2/\gamma^2 - ikr'\theta\sin\psi$$

$$-i(r'^2k/2\gamma^2R)]rdrd\psi \qquad \text{(I-56)}$$

(I-56) substituted into (I-43) yields for the power coupling coefficient the following

$$P = \frac{1}{2}\left(\frac{2}{\pi\omega a}\frac{WJ_0(U)}{VJ_1(U)}\right)^2\left\{\left[\int_0^{2\pi}\int_0^{\infty}\begin{pmatrix} J_0(Ur)/J_0(U) & r\leq 1 \\ K_0(Wr)/K_0(W) & r\geq 1 \end{pmatrix}\right.\right.$$

$$\left.\exp(-r'^2/\gamma^2)\cos(kr'\theta\sin\psi + r'^2k/2\gamma^2R)rdrd\psi\right]^2$$

$$+\left[\int_0^{2\pi}\int_0^{\infty}\begin{pmatrix} J_0(Ur)/J_0(U) & r\leq 1 \\ K_0(Wr)/K_0(W) & r\geq 1 \end{pmatrix}\right.$$

$$\left.\left.\exp(-r'^2/\gamma^2)\cos(kr'\theta\sin\psi + r'^2k/2\gamma^2R)rdrd\psi\right]^2\right\} \qquad \text{(I-57)}$$

To put P in the form (I-57), the coefficient a_p was expressed in

terms of its real and imaginary parts as follows

$$a_p = x + iy \tag{I-58}$$

Thus, the product $a_p a_p^*$ is given by

$$a_p a_p^* = x^2 + y^2 \tag{I-59}$$

CHAPTER II

MEASUREMENTS ON COUPLING AND ALIGNMENT SENSITIVITY

Measurements were made on the coupling of Gaussian beams into single mode optical Fibers. The measurements were performed to determine coupling efficiency and alignment sensitivity and verify the coupling and alignment sensitivity model. Measurements were made on coupling efficiency vs beam spot size, coupling vs lateral misalignment, coupling vs focal shift and coupling vs axis tilt. The measurements were performed at two wavelengths: 0.6328 micrometers from a helium neon (HeNe) laser and 0.8460 micrometers from a gallium aluminum arsenide (GaAlAs) laser.

Optical Fiber Preparation

The optical fibers used in the measurements were obtained from the Valtec Corporation. Single mode fiber for each of the above wavelength lasers was obtained. The fibers were coated with a few thousandths of RTV (a silicon based rubber) and had a loose outer jacket of stiff plastic with an inner diameter approximately 0.1 inches.

The fiber ends were terminated by epoxying the fiber ends into glass capillary tubes and polishing using standard techniques. A photo of a polished fiber end is shown in Figure 8. The design of the fiber termination is shown in Figure 9.

To polish a fiber end, the capillary tube with fiber was waxed into a hole in a glass plate and the plate then put on a polishing lap. The polished fiber ends were then examined for defects such as scratches. Two methods of examination were used.

The first examination was under a high magnification microscope to look for surface scratches and pits especially any near the core. Scratches the order of 0.25 micrometers could be observed. Considering that the core is about 6.0 micrometers, scratches larger than 1.0 micrometers could scatter sufficient light to affect coupling, Figure 10 shows photos of some of the polished fiber ends. All fiber ends polished were examined and photographed. The photographs were useful if fiber damage were suspected to have caused a change in performance of a fiber end's coupling ability.

The second examination of the fiber ends was performed with an interference microscope. This microscope is a miniature Michaelson interferometer with magnified view of the sample surface. This examination revealed irregularities in the surface contour. In

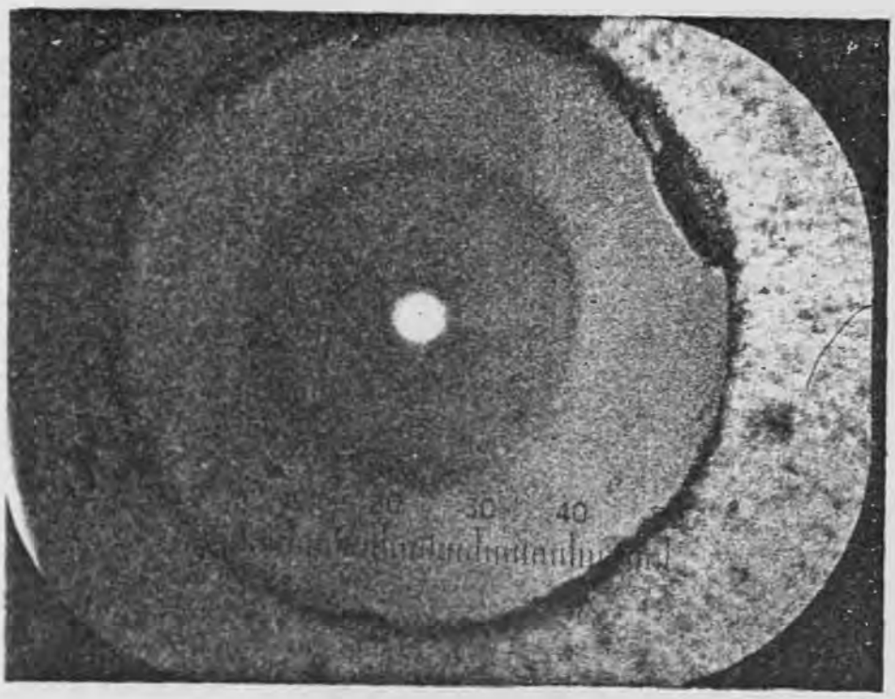

Figure 8. Polished end of a single mode optical fiber. The illuminated core is surrounded by the cladding. On the scale, each scale division is 1.25 micrometers.

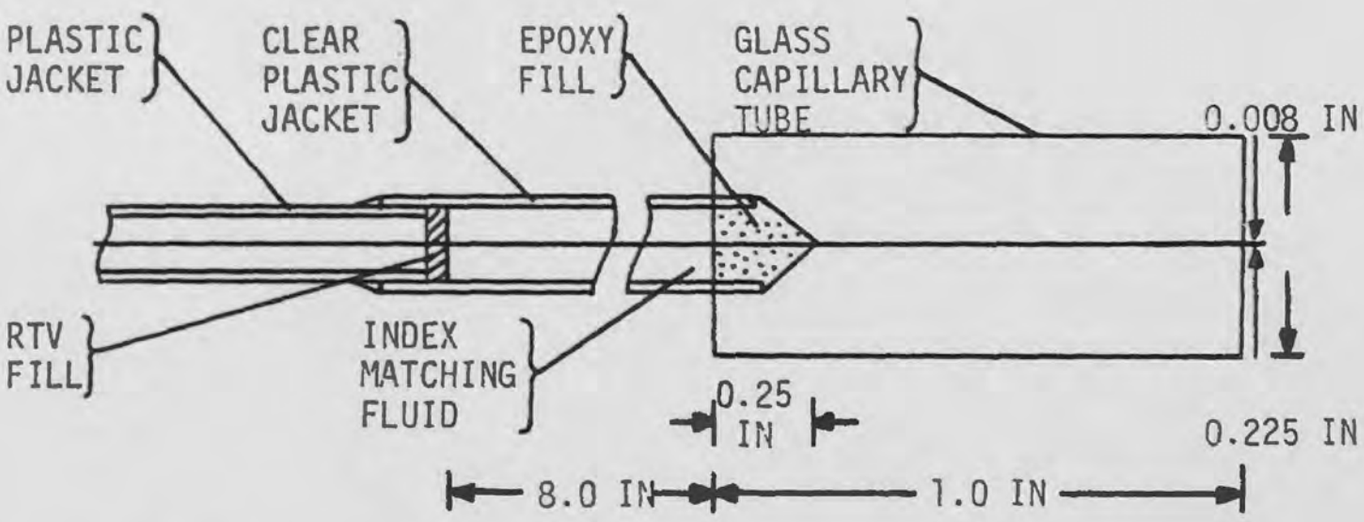

Figure 9. Single mode optical fiber cable termination design.

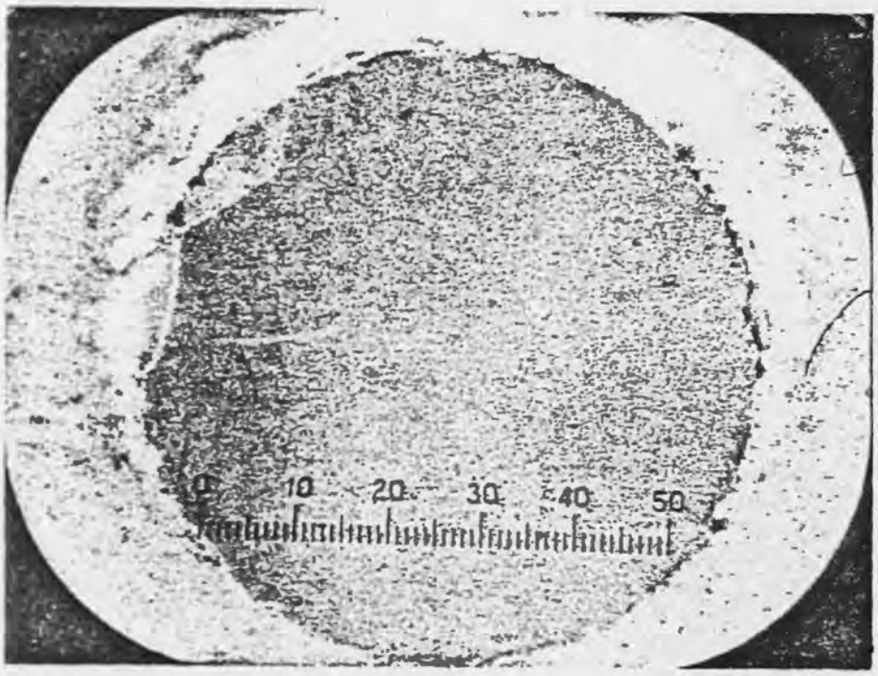

Figure 10. Example of polished single mode fiber. Epoxy surrounds the fiber. On the scale, each division is 1.25 micrometers.

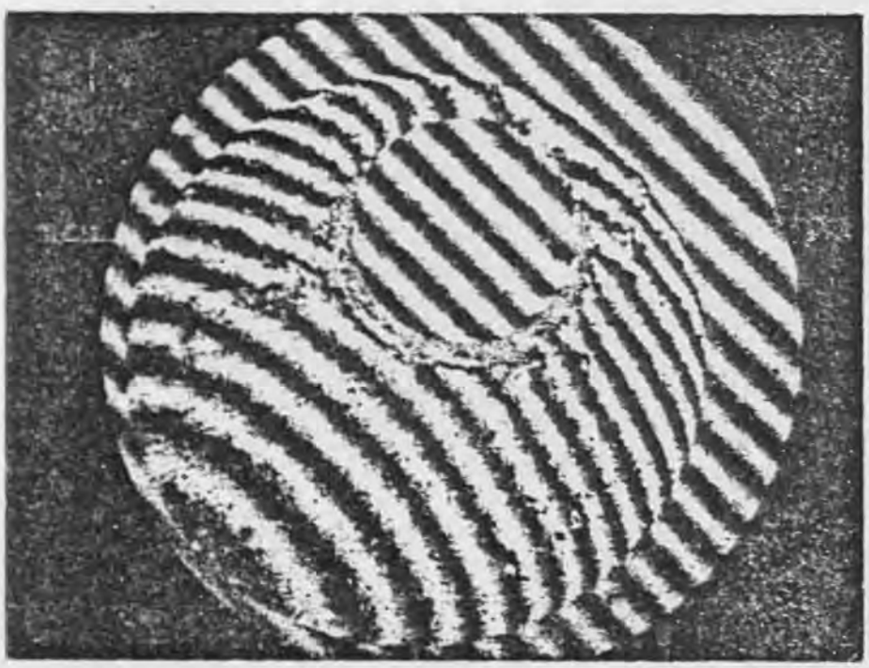

Figure 11. Example use of interference microscope. The distance between dark lines indicates a 0.27 micrometer change in height (half of the illumination wavelength). The magnification is 400X. The fiber is the same as in figure 10.

general, the fibers were flat to better than $\lambda/10$ at 0.54 micrometers. Photographs of fibers viewed on the interference microscope are shown in Figure 11. The fibers were viewed at an angle to produce fringes. As the fringe intensity goes from light to dark a change in height of $\lambda/4$ occurs.

The equally spaced fringes indicate a flat fiber end surface. Note that the epoxy is not as flat as the fiber since the fringes on the epoxy are not straight.

In all, five one meter length and one ten meter length fibers of each single mode fiber type were made into cables.

Measurement Setup

The light sources for the coupling experiments were a HeNe laser and a GaAlAs laser. The outputs of the lasers were passed through a spatial filter/collimator which removed stray light and adjusted the beam diameter. The beam diameter in combination with the coupling lens determined the focal spot size. The filtering was necessary for the GaAlAs laser since its output was multimode and emitted from a strip junction with length to height ratio of about 6:1. The HeNe laser output was in the fundamental Gaussian beam mode with some stray light present.

HeNe Laser Setup

The HeNe laser coupling setup is shown in Figure 12. The HeNe laser was initially aligned so that its beam was parallel within 1.0 milliradian to a bench upon which the components for performing the coupling were mounted. Next, the spatial filter/collimator was aligned so that its output beam was also parallel to the optical bench. Next, an optical isolator was mounted in the beam. The isolator was required since light reflected from the fiber end fed back to the laser, entered its cavity and caused output power fluctuations. The feedback was observed to cause periodic laser output power fluctuations the peaks of which exceeded the initial output by 10 percent. The isolator rotated the polarization of the reflected beam by 90°. The reflected beam was then rejected by a polarizer. The polarization rotation was performed by a quarter-wave plate placed after the above polarizer. The wave plate changed the polarization of the beam to circular polarization. Thus, light reflected from a fiber end again passed through the wave plate and became linearly polarized orthogonal to the laser output's polarization. The reflected light was rejected by the polarizer. All coupling data for single mode fibers for the HeNe laser was taken with this setup. What effect the use of circularly polarized light had different from using other polarizations was not considered. However, note that the two degenerate HE_{11}

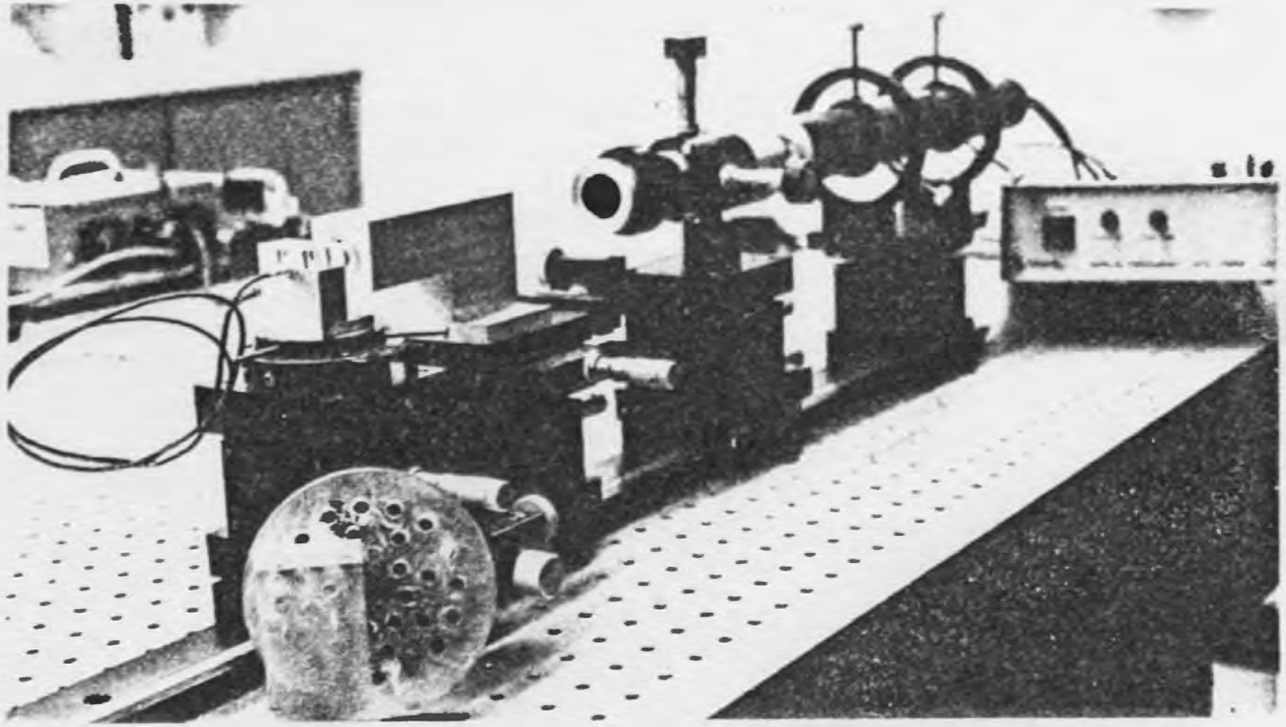

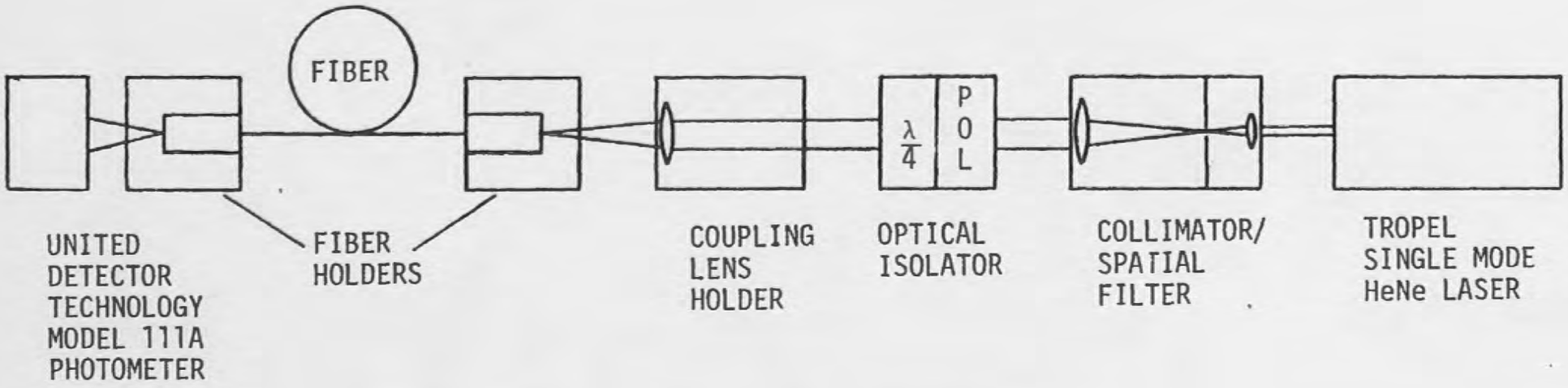

Figure 12. Fiber optic coupling test set-up.

waveguide modes have orthogonal linear polarizations, thus, both modes were possibly excited.

Next, the fiber was mounted and adjusted so that the laser beam was on the fiber end.

Next, the fiber was tilted to compensate for deviation in the end face angle. Compensation for the angle of the fiber end with respect to the fiber axis is necessary for efficient coupling. Some fiber faces had small angles by accident while on others a 5° angle was purposely produced. The angled fiber face was tested as a means for preventing reflected light from returning to the laser. The correct fiber alignment when the end is not 90° to the fiber axis is discussed below.

The alignment procedure was to rotate the fiber about its axis until the reflected light was in a plane parallel to the plane of the optical bench. The angle of deflection from the input light beam was measured using a convenient triangle. Next, the fiber was rotated about its axis 180°. The reflected light again lay in a plane parallel to the plane of the optical bench. The angle with respect to the input light beam was measured. The average of these two angles is twice the fiber face angle. The difference of these two angles is twice the fiber mount angular error.

The angle at which the fiber axis is set with respect to the input light beam axis is given by a geometric analysis of how the fiber acceptance cone is affected by an angled end face. The analysis is straight forward and requires use of Snell's law and the expression for the critical angle.

$$\text{Snell's Law:} \quad n_1 \sin\theta_1 = n_2 \sin\theta_2 \tag{II-1}$$

$$\text{Critical angle:} \quad \Phi_c = \sin(n_1/n_2) \tag{II-2}$$

The incoming light is traced by Snell's law through the dielectric boundary at the air/optical fiber interface. Figure 13 shows the geometry. Rays interior to the fiber which exceed the critical angle escape the fiber. Rays which are at angles less than the critical angle are total internally reflected and waveguide through the fiber. This is a simple geometric picture of the fiber acceptance cone angle size and waveguide condition. The expression for the axis angle ψ is given by:

$$\psi = (\alpha_1 + \alpha_2)/2 \tag{II-3}$$

Where α_1 and α_2 are proportional to the external critical angles associated with incident light rays above and below the axis. See

Figure 13. The angles α_1 and α_2 are related to the external critical angles by the following expressions.

$$\alpha_1 = \theta_{c1} - \beta$$
$$\alpha_2 = \theta_{c2} - \beta \qquad \text{(II-4)}$$

Where θ_{c1} and θ_{c2} are the external critical angles given by

$$\sin\theta_{c1} = \sqrt{n_1^2 - n_2^2}\cos\beta + n_2\sin\beta \qquad \text{(II-5)}$$

and

$$\sin\theta_{c2} = \sqrt{n_1^2 - n_2^2}\cos\beta - n_2\sin\beta \qquad \text{(II-6)}$$

Next, the coupling lens was mounted and adjusted so that the input light beam falls upon the fiber end. Because the beam had been previously centered upon the fiber, the lens did not change the angle of the beam axis with respect to the fiber axis. At this point a photometer was inserted between the lens and the fiber. The power transmitted by the lens, P_{lens}, is measured. The power P_{lens} was also the light flux on the fiber end surface.

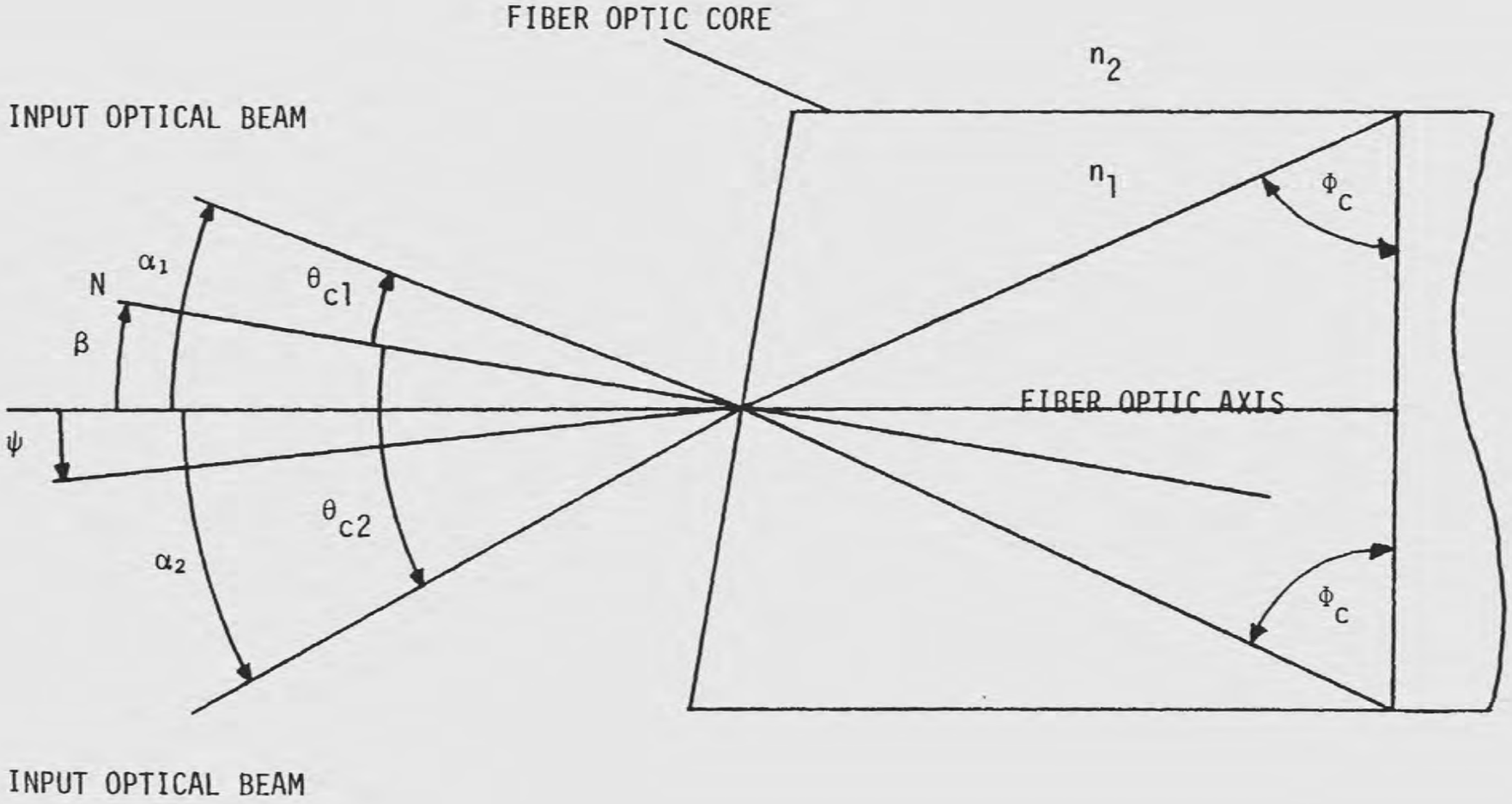

Figure 13. The fiber's light acceptance cone axis location when the fiber face is slanted at angle β with respect to the optical fiber axis.

Next, light was coupled into the optical fiber. The fiber was adjusted using micropositioners. To aid the initial alignment, a low powered microscope was used to observe the fiber end. To obtain some initial coupled light, the fiber end was set away from the beam focus. The light power, P_{fiber}, exiting the opposite fiber end was collected by the photometer. Adjustments on the positioners was continued untill no further increase in light throughput was obtained. The efficiency of the fiber was computed from the following formula.

$$P = \frac{P_{lens} - P_{Bkg}}{P_{fiber} - P_{Bkg}} \qquad \text{(II-7)}$$

Where P_{Bkg} is the insitu background power reading on the photometer.

GaAlAs Laser Set

The GaAlAs laser consists of a PN junction in a doped single crystal of GaAs into which a double strip diffusion forms the junction. Hence, the name double heterojunction commonly referred to as the DHJ laser. Current is passed through the junction to create free carriers which return to the valence band by emitting a photon of light whose wavelength is determined by the junction energy gap.

The cavity is formed by cleaving the crystal along planes perpendicular to the junction. The junction geometry is typically 2.0 micrometers high and 13.0 micrometers wide producing a 6:1 aspect output beam. This beam will inefficiently couple to a round single mode optical fiber. Smaller aspect ratio diode lasers are being developed, fortunately.

For fiber coupling experiments, a TEM_{00} Gaussian beam was desired. The approach taken to reshape the beam from the GaAlAs laser was the following. A 16mm focal length microscope objective lens was used to collimate the output. Then the spatial filter collimator was used to circularize the beam. The collimator adjusted the beam size. Beams with close to Gaussian shape were obtained.

No isolator was used with the coupling setup. Isolation was not needed. The GaAlAs laser has a high gain medium, thus, power removed by reflected light has much less affect on the GaAlAs laser than on the HeNe laser which has a low gain medium. In all other respects the two coupling setups were the same.

Beam Spot Size

The input beam diameter and coupling lens focal spot diameter were measured to correlate spot diameter to coupling. The input

beam diameters were measured using a scanned knife edge. The knife edge scan gives the profile of the integrated power in the exposed beam. The formula for integrated power is obtained by integration of the Gaussian beam expression. The result is the normal distribution function.

$$P(x \leq x_o) = P_o\left[\frac{1}{2} + \frac{2}{\sqrt{2\pi}\omega}\int_0^{x_o} \exp(-2x^2/\omega^2)dx\right] \qquad \text{(II-8)}$$

The beam spot diameter was obtained by determining the values of x_o for which $P(x \leq x_o)$ is equal to 0.16 and 0.84. At these points $x_o = \pm\omega/2$. Thus, the distance between these positions is the beam radius. The beam shape can be recovered by differentiation of the measured data. The collimator lenses and measured beam diameters used in the coupling experiments are shown in Table 1. Each line in the table gives the beam parameters for each coupling setup used.

The focal spot sizes in Table 1 were measured using pinholes placed at the beam focus. The fraction of power passing through the pinhole was measured and the diameter of a Gaussian beam

TABLE 1 COUPLING BEAM SPOT DIAMETER

LASER SOURCE	COLLIMATOR LENSES(mm) PRIMARY	SECONDARY	BEAM DIAMETER (mm)	COUPLING LENSES f (mm)	BEAM f/#	SPOT SIZES (μm) MEASURED 6.3μm PIN HOLE	MEASURED 11.3μm PIN HOLE	PLANE WAVE	GAUSSIAN WAVE	COUPLING BEAM NUMBER
HeNe	16	80	4.7		4.7	11.0 10.7 10.8	16.1 16.5 16.3	21.0	1.9	1
	30	80	2.7	22	8.2	10.0 10.1 10.0	10.4 10.5 10.4	15.2	3.3	2
	46.8	80	1.9		12	12.6 12.0 12.3	14.0 12.6 13.3	18.8	4.7	3
	80	80	1.02	7	6.7	12.2 8.3 10.2	16.4 11.9 14.1		2.76	4
GaAlAs	30	80	3.02		7.3	15.0	15.7	18.7	3.92	5
	46.8	80	2.36		9.3	16.1	16.2	21.0	5.02	6

which would pass the same fraction determined from the following equation for the power in the pinhole diameter.

$$P\ (r \leq r_o) = P_o\ [1-\exp(-2r^2/\omega^2)] \qquad \text{(II-9)}$$

Where P is the power passed by a pinhole having radius r_o and an incident beam of radius ω. To improve the reading accuracy two pinhole sizes were used. The two pinhole sizes revealed when the beam deviated from the Gaussian shape. For low F-numbers the beams were non-Gaussian due to spherical aberration.

Also shown in Table 1 are the spot diameters, 2ω, predicted by Gaussian beam optics (no limiting apertures) and the spot diameter, s, including spherical aberration and diffraction given by (Smith 1966).

$$s = 2\left(\frac{K(n)\ D^3}{2F^2} + \frac{1.22\lambda F}{D}\right) \qquad \text{(II-10)}$$

Where K(n) is a factor determined by the curvature of the lens' surfaces and the lens substrate's refractive index n. D is the beam

diameter and F is the lens focal length. The first term on the right is the spherical aberation contribution to the spot diameter. The second term on the right is the diffraction contribution to the spot diameter. Equation (II-10) is strickly correct for plane waves with flat intensity profiles, which may account in part for the measured diameters being significantly different.

The Gaussian beam spot diameter using (I-4) is given by:

$$2\omega_0 = 2F\lambda/\pi D \qquad \text{(II-11)}$$

One observation from the table can be made about the two lenses. (Both lens are of minimum spherical aberration design (Jenkins 1957) and made to the same tolerances). The shorter focal length, 7mm, lens has more aberration as evidenced by the larger spot calculated measuring with the large pinhole than that calculated measuring with the small pinhole. This indicates the light distribution is more peaked in the center or has more power in the skirt than a Gaussian spot. For the F/8.1 and F/11.6 beams the 22mm focal length lens produced focal spots which were very close to Gaussian shape as evidenced by the two pinhole measurements of spot diameter being near equal.

Numerical Aperture

The numerical aperture (NA) is defined as the quantity $\sqrt{n_1^2-n_2^2}$. From either (I-64) or (I-65) the external critical angle, θ_c, for a fiber with end face at a right angle to its axis is given by:

$$\sin\theta_c = \sqrt{n_1^2 - n_2^2} \qquad \text{(II-12)}$$

Thus, the sine of the critical angle is equal to the NA of the fiber. The critical angle defines the geometric angular limits at which light rays may enter into a fiber and be waveguided. Thus, the NA gives information about the coupling properties of an optical fiber.

NA of optical fibers is measured usually by measuring the cone angle of light emitted by a fiber. This technique was used here. The approach is to determine the beam diameter at two positions along the beam axis in the far field. The beam cone angle is given by:

$$\theta_{cone} = \tan^{-1}[(\omega_2 - \omega_1)/(L_2 - L_1)] \qquad \text{(II-13)}$$

Where ω_1 and ω_2 are the beam radii defined at the 90% contained power points. L_1 and L_2 are the beam axis positions at which the measurements are made. θ_{cone} is very close to the critical angle given by (I-12).

Coupling Efficiency

The polished single mode optical fibers were mounted in the setup shown in Figure 12 and the input beams described in Table 1 were used to measure coupling efficiency. In addition, the numerical aperture, core diameter and cladding diameter were measured. These and other fiber data are presented in Table 2. The coupling efficiency of single mode fibers for the wavelengths 0.6328 micrometers and 0.8460 micrometers were measured versus coupling beam focal spot diameter. The data are shown in Table 3. The fiber cable designations are coded as follows. SM is single mode, 6328 and 8200 are the single mode design wavelengths (the wavelength actually used for the 0.8200 micrometers fiber was slightly different). The next number is the angle of the fiber end face normal to the fiber axis. The next designation refers to the fiber cable length and finally the fibers of the same design wavelength and cable length are numbered. Two fibers with ends angled near 5

TABLE 2 CHARACTERISTICS OF THE SINGLE MODE FIBERS

Parameter	Fiber 1	Fiber 2
Single mode wavelength	0.6328 μm	0.8460 μm
Core diameter	6.0 μm	6.6 μm
Cladding diameter	70.5 μm	83 μm
Core refractive index	1.453	1.453
Numerical aperture	0.063	0.079
Normalized frequency, V	1.930	1.946
Fresnel reflection loss		
Per surface (measured)	0.034	0.034

TABLE 3 COUPLING EFFICIENCIES

FIBER CABLE NUMBER	END	COUPLING EFFICIENCY FOCAL SPOT DIAMETER (μm)					
		16.3	10.4	13.3	14.1	15.7	16.2
SM6328 <2.0 , 1.0m #0	1	46.7	73.3	62.3	76.5		
SM6328 <2.29 , 1.0m #0	2		71.1				
SM6328 <1.3 , 1.0m #1	1	48.4	78.9	67.1	75.8		
SM6328 <3.05 , 1.0m #1	2	51.0	79.7	65.8	77.7		
SM6328 <0 , 1.0m #2	1			71.0			
SM6328 <2.25 , 1.0m #2	2	40.0	70.0	63.7	61.7		
SM6328 <2.77 , 1.0m #5	1	43.1	65.2	57.7	59.6		
SM6328 <1.48 , 1.0m #5	2	41.2	65.0	53.3	63.3		
SM6328 <5.1 , 1.0M #2	1	50.5	83.2	71.0	74.3		
SM6328 <2.86 , 1.0m #2	2	48.5	83.8	73.6	71.3		
SM6328 <4.87 , 1.0m #1	1	49.3	78.9	63.6	70.6		
SM8200 <1.3 , 1.0m #1	1					53.7	61.0
SM8200 <0.37 , 1.0m #1	2					68.9	66.0
SM8200 <0.25 , 1.0m #2	1					69.7	66.1
SM8200 <0.13 , 1.0m #2	2						64.9
Mean		47.3	74.9	64.9	70.1	64.0	64.5
Standard Deviation		3.5	7.0	6.3	6.8	9.0	2.4
CALCULATED		64.4	87.2	75.7	72.3	69.4	67.5

degrees are numbered separately as #1 and #2 in the SM6328 category.

The computed coupling predictions were determined using (I-44) and an assumed transmission at the entrance and exit faces of the fiber of 0.93 due to Fresnel reflection loss at the air/fiber interface. Figures 14 and 15 show plots of coupling efficiency vs beam spot diameter calculated from (I-44). Also shown are experimental data and data error bars.

The original plan was to have fibers with only two end face angles: 0 degrees and 5 degrees. The glass capillary tubes varied in size enough that some fit loosely in the polishing blank during waxing into the blank resulting in an angled end face. The data reveal no obvious effect of an angled fiber end. The general behavior shows slightly better coupling was achieved with the fiber faces having larger angles. The data do reveal that coupling depends upon spot diameter.

Alignment Sensitivity

The sensitivity of fiber coupling to misalignment of the beam axis and the fiber acceptance cone axis was measured for three degrees of freedom described in Chapter I. For each alignment

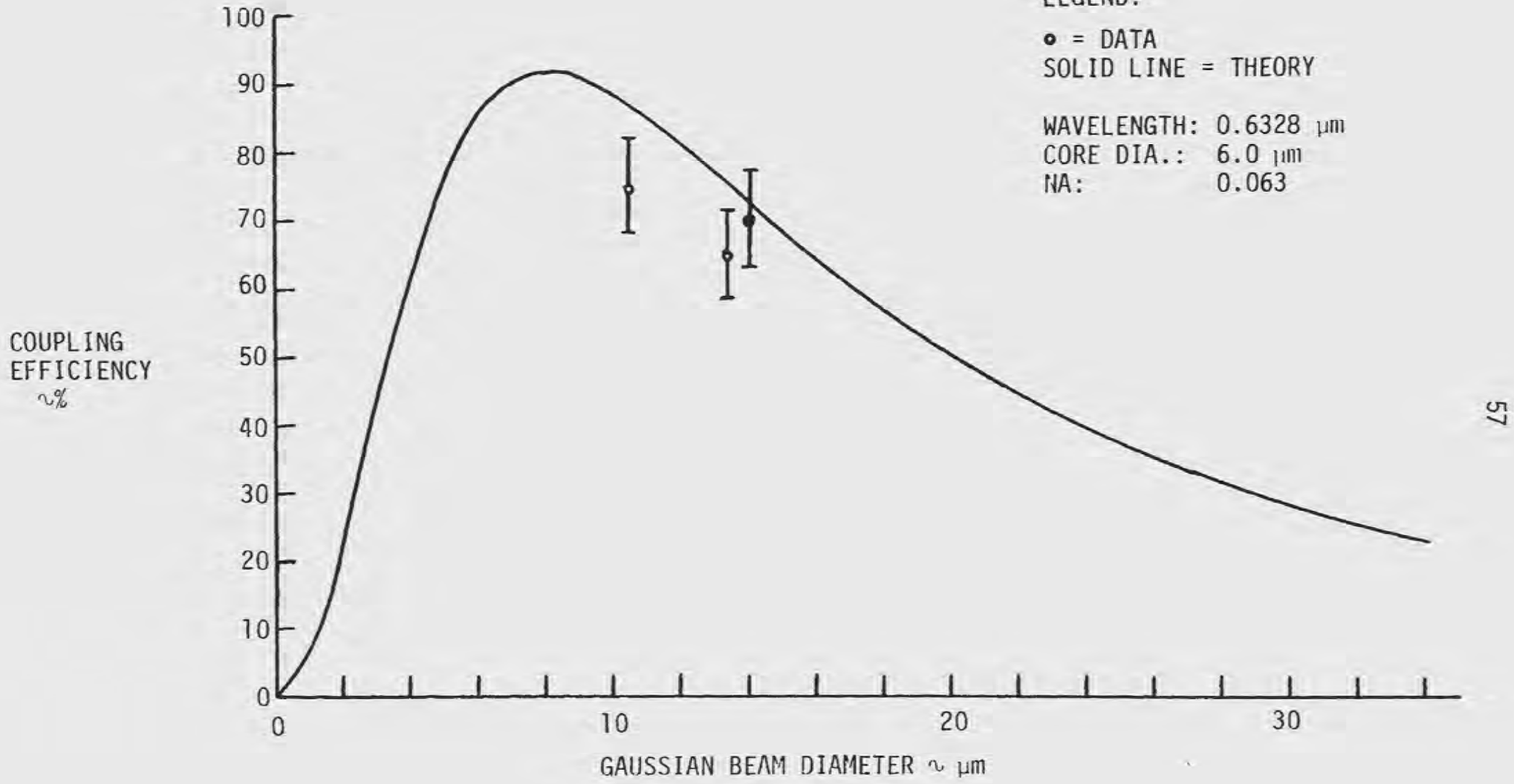

Figure 14. Single mode fiber coupling efficiency versus spot size for the HeNe laser.

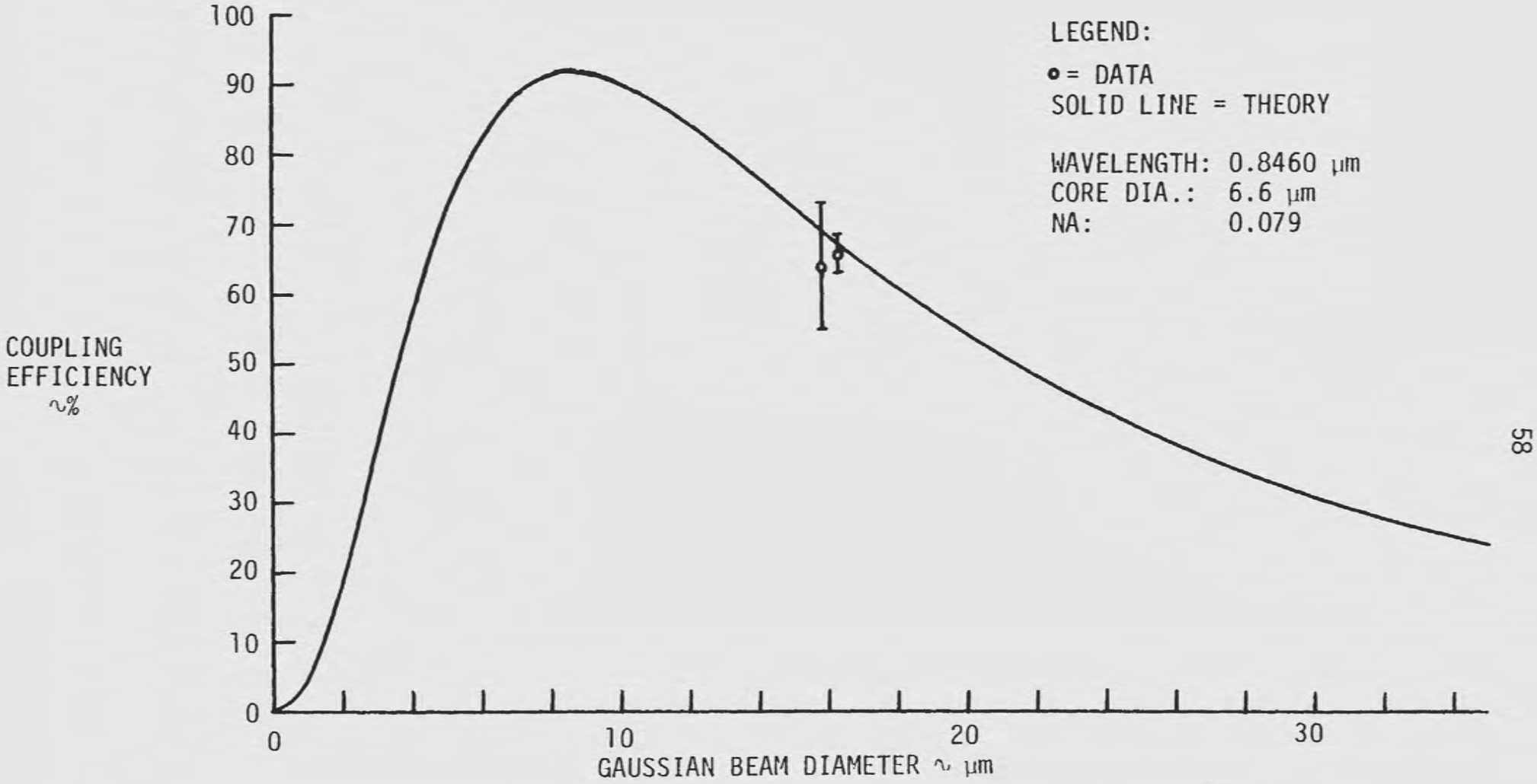

Figure 15. Single mode fiber coupling efficiency versus spot size for the GaAlAs laser.

sensitivity all other alignments remained fixed at settings for peak coupling efficiency. The coupling versus misalignment curve was recorded for two fibers selected from Table 3. The results are shown in Table 4 along with calculated values using the sensitivity models of Chapter I. Figure 16, 17 and 18 show typical plots of alignment sensitivity curves for the single mode fiber at 0.6328 micrometers wavelength. Both the calculated and experimentally determined curves are shown.

The predicted coupling for focal shift misalignment requires knowledge of the variation of spot diameter with focal shift. What is required is the spot diameter between the lens and the focus. The spot diameters at these two points are given in Table 1. (I-4) gives the desired relationship for purely Gaussian beams. In the following a modified expression is developed which fits the spot diameters measured at the lens and focal point. (I-4), for the Gaussian beam spot radius, can be rewritten.

$$\omega(z) = \sqrt{\omega_0^2 + (\lambda z/\pi\omega_0)^2} \qquad \text{(II-14)}$$

At $z=0$ $\omega(o) = \omega_0$ according to (II-14). At z large (II-14) is

TABLE 4. ALIGNMENT SENSITIVITY VERSUS COUPLING BEAM.

		MISALIGNED COUPLING 3dB WIDTH					
LENS FOCAL LENGTH (mm)	BEAM NUMBER	LATERAL (μm)		FOCAL SHIFT (μm)		ANGULAR (mrad)	
		THY	EXP	THY	EXP	THY	EXP
22	1	10.8	5.25±0.3	107	185±10	60.0	117±1
22	2	7.96	6.7±0.1	162	252±3	73.2	98±.2
22	3	9.48	8.4±0.1	243	425±25	65.2	85±1
7	4	9.92	6.4±0.6	146	225±5	63.6	123±15
22	6	11.1	9.4	217	300	78.0	60

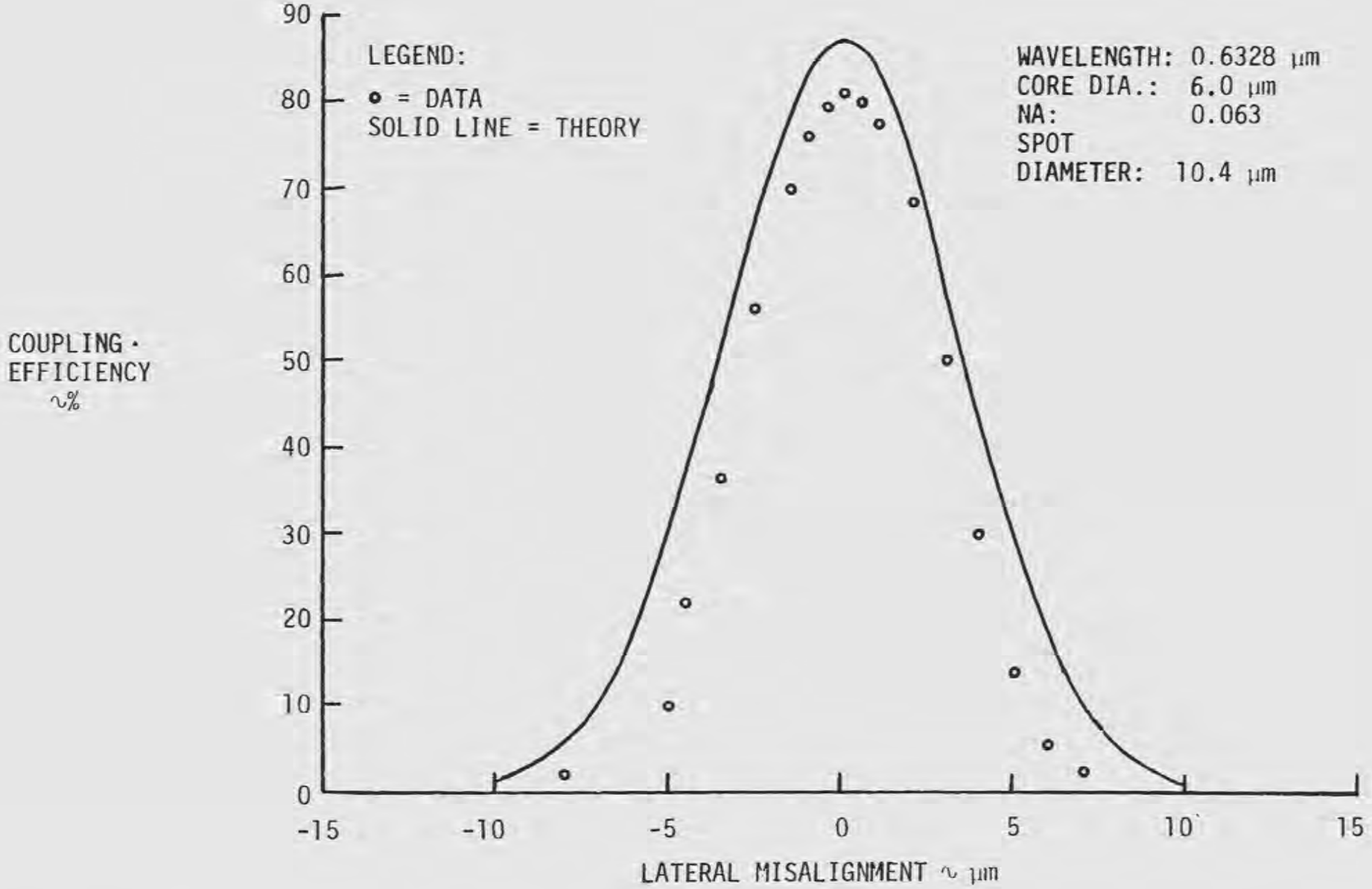

FIGURE 16. Single mode fiber coupling efficiency versus lateral misalignment for the HeNe laser.

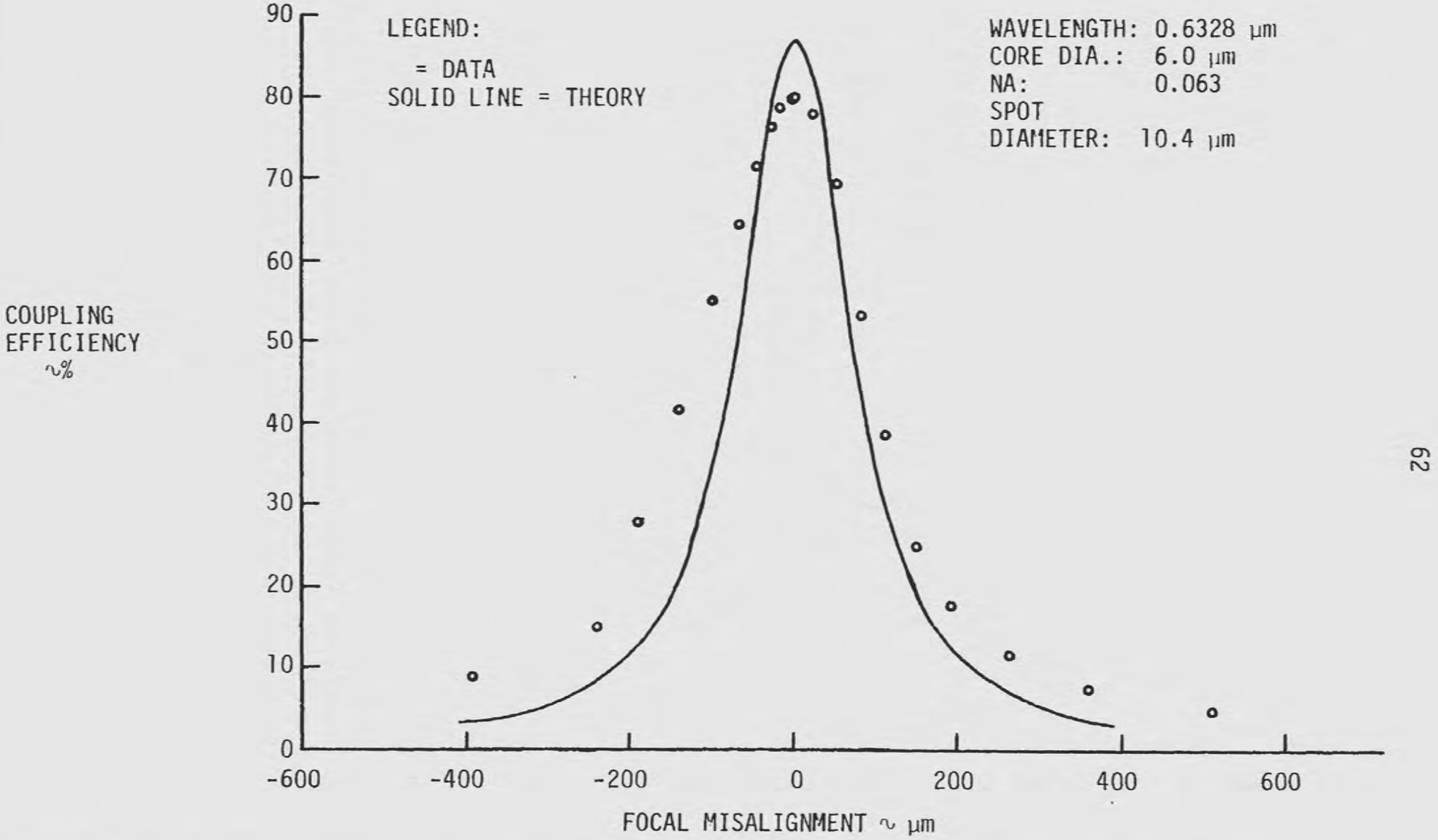

Figure 17. Single mode fiber coupling efficiency versus focal misalignment for the HeNe laser.

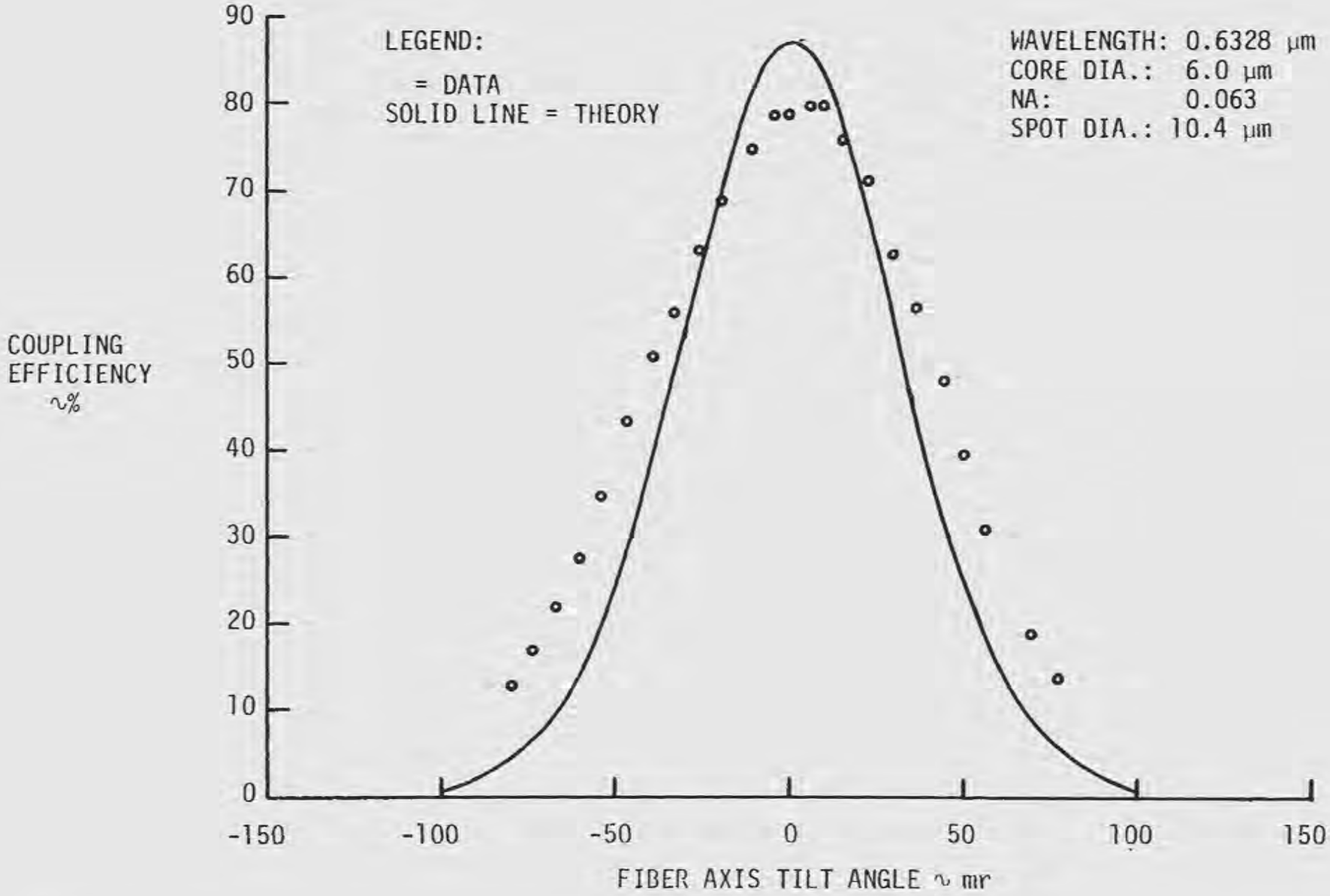

Figure 18. Single mode fiber coupling efficiency versus fiber axis tilt for the HeNe laser.

asymptotic to the following expression:

$$\omega(z) = \lambda z/\pi\omega_0 \quad \text{For } z \text{ large.} \qquad \text{(II-15)}$$

(II-15) was used to obtain the Gaussian focal spot radius produced by a beam of given diameter at a lens of focal length, F, and was used to obtain the Gaussian focal spot diameters listed in Table 1.

(II-14) can be modified to give the correct focal spot radii if in the first term on the right side ω_0 is replaced by ω_0' , the measured spot radius. The new expression for the beam radius is given by:

$$\omega(z) = \sqrt{\omega_0'^2 + (\lambda z/\pi\omega_0)} \qquad \text{(II-16)}$$

Figure 19 shows a plot of spot diameter predicted by (II-16) (twice the spot radius of (II-16)) and measurements with a pinhole. (II-16) was used to perform the focal shift misalignment predictions.

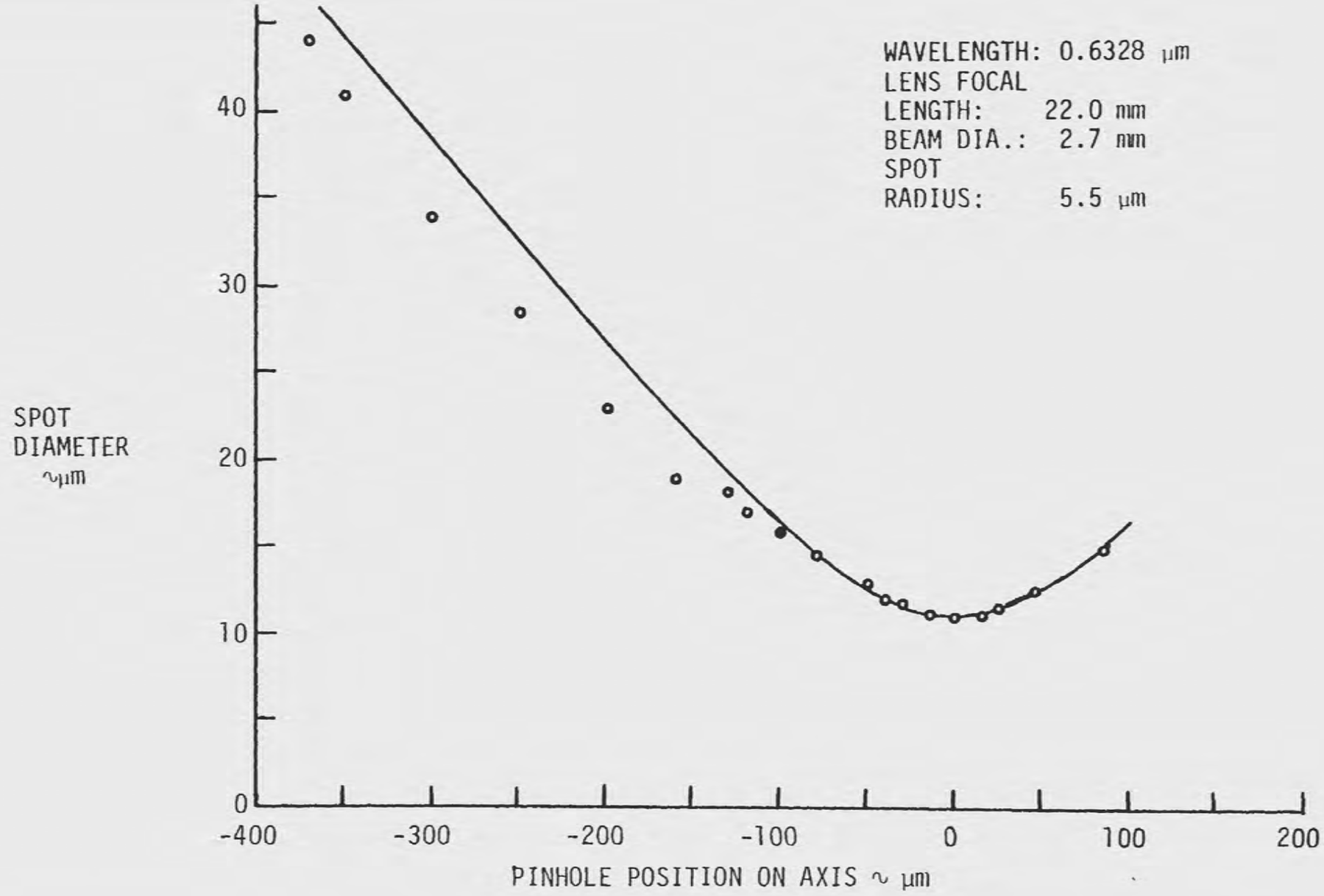

Figure 19. Coupling beam diameter near the focus versus position on the beam axis. The beam parameters are those of beam 1 (See Table 1.)

CHAPTER III

CONCLUSIONS

In Chapter I, models are presented which predict coupling efficiency and alignment sensitivity for single mode optical fibers. The expressions used to describe the fiber optic modes were developed by Snyder (1969a). He performed asymptotic expansions of the eigenfunction and eigenvalue equations in terms of u_p/k and retained only zero order terms. He obtained simple expressions for the eigenfunction and eigenvalue equations. The expressions obtained are valid for single mode optical fibers such as those investigated in this work. One requirement is that δ defined by (I-26) be much less than one. The fibers investigated in this work have δ values near 0.002.

Next, a fiber coupling efficiency model was derived assuming linear superposition and orthogonality of the fiber modes. An expression for the coupling of a fundamental mode Gaussian beam into the fundamental fiber optic waveguide mode was obtained similar to the expression given by Stern (1970). In addition, models for the effects on coupling of three misalignments were developed: lateral misalignment of the fiber in the coupling lens' focal plane (after Stern

(1971)), displacement of the fiber along the beam axis (or focal shift), and angular misalignment of the fiber axis with respect to the beam axis (after Imai (1973)).

Experimentally, optical fiber coupling and alignment sensitivity were measured on two single mode optical fibers having different cut-off wavelengths. Light beams having a fundamental mode Gaussian shape were used in the measurements.

Coupling Efficiency

Coupling efficiency measurements were made versus coupling beam F-number. The coupling model includes only the focal spot size. However, as shown in Table 1, the power distribution in the focal plane is a function of the lens' aberrations, which in turn are functions of the coupling beam F-number. For small F-numbers (<6), spherical aberration is significant and alters the Gaussian beam such that the intensity profile in the focal plane is non-Gaussian. The coupling results shown in Table 3 show that lowest coupling occurred for the smallest F-number beam. For larger F-numbers (>6), the spherical aberation is small and at the focal plane the coupling beams had Gaussian profiles. For large F-numbers, the diffraction spreading of the coupling beam due to the lens aperture can be significant. This

contribution to the spot size was reduced by selecting a lens diameter significantly larger than the beam diameter.

The best coupling was obtained with the smallest diameter focal spot. The predicted limit on the spot size for efficiency coupling as seen from Figures 14 and 15 is about 8.0 micrometers or about 2.7 core diameters. The safe approach to good coupling efficiency is to use large F-numbers, since less deviation from a Gaussian beam profile is obtained. The data indicate that deviation from the Gaussian profile affects coupling more than the beam diameter.

Alignment Sensitivity

Alignment sensitivy measurements were made versus coupling beam F-number. Here, too, the model contains only spot sizes. Aberrations in the focused beam certainly affected the results, but to what extent was not determined.

Lateral Misalignment

The lateral misalignment predicted full width at half maximum (FWHM) or -3dB width was slightly larger than measured widths as shown in Table IV. Here the result for the F/8 beam came closest to prediction.

This misalignment measurement was easiest and was least prone to error. As to be expected, a large beam diameter reduces lateral alignment sensitivity. The sensitivty of coupling to lateral displacement was the greatest of the three misalignments investigated. The predicted coupling versus misalignment curve is similar to experiment as shown in Figure 16.

Focal Misalignment

The predicted FWHM for focal shift misalignment in all cases was smaller than measured. Here, there were several possible error sources. The beam size data needed for the coupling prediction versus focal shift had to be model as discussed in Chapter II. This model contributed additional uncertainty. A second possible factor was the effect of cladding light, which would tend to increase coupling. A mode stripping test was performed on these fibers. The test showed that the cladding light contribution for 1.0 meter of fiber was less than 1 percent. This result appears to discount as an error source the contribution due to cladding light.

In Figure 20, the focal shift misaligned coupling for beams 1 and 3 are shown. The results for beam 2 are shown in Figure 17. In all three cases, the curve shapes of the experimental data are similar to the theoretical model data. One interesting feature of

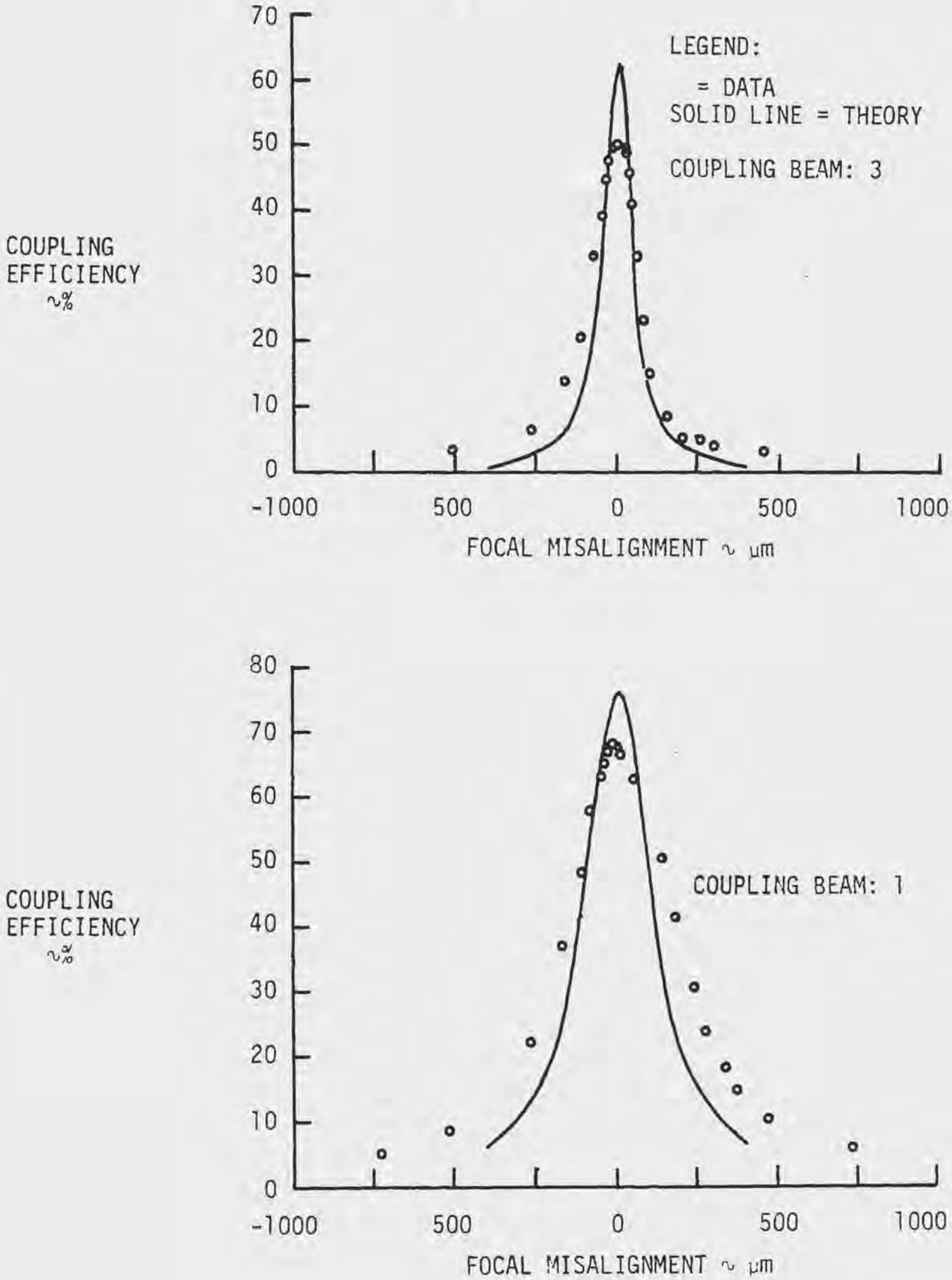

Figure 20. Single mode fiber coupling efficiency versus focal misalignment for the HeNe laser.

these curves is the behavior near their peaks. The experimental curves are not as sharply peaked. The indication is that the coupling conditions are more critical near the focus. Thus, the experimental coupling differed from the model the most near the peak due to non-ideal conditions. That is, residual amounts of each misalignment were present causing a loss of coupling. Thus, the predicted FWHM's are narrower in part due to the curve being more sharply peaked than the experimental data. The fit of the model to the data is better than a comparison of FWHM's would indicate.

Another source of error in the model is the assumption of Fresnel reflection for normal incidence for all misalignments. Significant error could occur near the focus where phase front curvature reaches a minimum. (At the focus the phase front is flat.) Thus, near the focus off-axis light rays may be propagating at large angles with respect to the beam axis. The effect of incidence angle on reflection at a dielectric interface is described by Fowles (1968). There, the reflectance is shown to be relatively constant for ray angles up to 30 degrees. For larger angles, the reflectance increases until at 90 degrees(grazing incidence) the reflectance is unity. The behavior of the TE and TM polarization components of the incident light is similar except near Brewster's angle (about 44 degrees for quartz) at which the TM component's reflectance is zero.

The angle of rays with respect to the beam axis can be defined

by the phase front curvature, R. If the ray angle is Γ, then the sine of Γ is given by

$$\sin\Gamma = \rho/R \qquad \text{(III-1)}$$

Where ρ is the radial position. Significant coupled light is obtained within a radial distance of about 10 micrometers. (See the discussion in Chapter II under Tilt Misalignment.) R can be shown to reach a minimum of about 100 micrometers in the near field. Thus, for light rays which couple into the fiber, Γ could be the order of 10 degrees according to (III-1) and using the above values of ρ and R. For an angle of 10 degrees the Fresnel reflectance is not too different from its value for on-axis light rays. By this simple analysis, it appears that increased reflection loss due to the curvature of the beam phase front in the near field is not a major source of error in the coupling model.

Tilt Misalignment

The model predictions shown in Table 4 of the coupling FWHM's are smaller than those obtained experimentally. One reason may be that at the fiber the coupling beam phase front was not flat. (The model assumed that the phase front was flat at the fiber.) To test this theory, the computer code of the model was run with the radius of curvature of the phase front set at 1000 and then 100 micrometers. The results are shown in Table 5 for coupling beams 1, 2, and 3.

TABLE 5

Effect of Radius of Curvature on the Coupling FWHM(mr)

BEAM NUMBER	THEORY			EXPERIMENT
	R=∞	R=1000μm	R=100μm	
1	60.0	60.6	86.0	117
2	73.2	73.4	87.8	98
3	65.2	65.6	86.0	85

Obviously, radius of curvature has an effect from the results shown in the Table. Study of the Gaussian beam phase term provides the answer. The curved phase front rolls across the fiber face with tilt angle such that the phase mismatch gets no worse. The peak coupling is reduced. This simple picture indicates phase front curvature may have affected the results of the experiment.

Another influencing factor may be the focal plane energy distribution of the coupling beams. For small F-number, the distribution is determined by the spherical aberration, while for large F-number, the energy distribution is determined by diffraction by the lens aperture.

In conclusion, this paper has shown that the theoretical models for coupling efficiency and alignment sensitivity of single mode optical fibers can predict the fiber's performance reasonably well.

APPENDIX

The wave equation is derived from Maxwell's equation in a homogeneous charge-free medium in which no currents are present. The maxwell equations take the following form for the conditions described.

$$\nabla \times \vec{H} = \varepsilon \partial E/\partial t$$

$$\nabla \times \vec{E} = -\mu \partial H/\partial t \qquad (1)$$

Where H is the magnetic field strength in Ampere/meter, E is the electric field strength in Volts/meter, ε is the electric permittitivity if Farad/meter, μ is the magnetic permeability in Henry/meter, t is time and ∇ is the del operator.

Taking the curl of the second expression and substituting the first expression in the curl of the second yields

$$\nabla \times \nabla \times \vec{E} = -\mu \partial(\nabla \times \vec{H})/\partial t$$

$$\nabla(\nabla \cdot \vec{E}) - \nabla^2 \vec{E} = -\mu\varepsilon \partial^2 \vec{E}/\partial t$$

For a charge free medium, $\nabla \cdot \vec{E} = 0$,

thus, the result is

$$\nabla^2 \vec{E} - \mu\varepsilon \partial^2 E/\partial t = 0 \qquad (2)$$

Which is the wave equation. For a monochromatic wave, a harmonic dependence in time can be assumed of the form

$$\vec{E} = \mathrm{Re}[\vec{E}(x,y,z)\exp(i\omega t)] \tag{3}$$

Thus, (2) can be written

$$\nabla^2\vec{E} + k^2\vec{E} = 0 \tag{4}$$

$$k^2 = \omega^2\mu\varepsilon \tag{5}$$

Gaussian Beams

Assume a solution whose transverse dependence is on r only so that ∇^2 can be replaced by

$$\nabla^2 = \nabla_t^2 + \partial^2/\partial z^2 \tag{6}$$

The problem symmetry is cylindrical so that a cylindrical coordinate system is appropriate. In cylindrical coordinates, the transverse Laplacian is given by

$$\nabla_t^2 = \frac{\partial^2}{\partial r^2} + \frac{1}{r}\frac{\partial}{\partial r} + \frac{1}{r^2}\frac{\partial}{\partial \theta^2} \tag{7}$$

Assuming no azimuthal variation of the wave equation gives for ∇^2 the following

$$\nabla^2 = \frac{\partial^2}{\partial r^2} + \frac{1}{r}\frac{\partial}{\partial r} + \frac{\partial^2}{\partial z^2} \tag{8}$$

For nearly plane wave propagation in which the flow of energy is predominately along a single axis, the z axis, only a single transverse field component is needed. Thus, (4) can be reduced to scalar form. Assume the value for E is

$$E = \psi(x,y,z)\exp(-ikz) \tag{9}$$

Thus, (4) becomes using (6) and (9)

$$\nabla_t^2 E + \partial E/\partial z^2 + k^2 E = 0$$

$$\nabla_t^2 \psi - i2k\partial\psi/\partial z + \partial^2\psi/\partial z^2 = 0 \tag{10}$$

Next, apply the condition that the field varies slowly along z so that

$$\partial^2\psi/\partial z^2 << k\partial\psi/\partial z$$

Thus, (10) becomes

$$\nabla_t^2 \psi - i2k\partial\psi/\partial z = 0 \tag{11}$$

Equation (11) is the form of the wave equation used to obtain the Gaussian beam solution.

Guided Waves

For waves in a circular dielectric rod, the wave equation (4) is expressed in cylindrical coordinates with the z axis variation assumed small (negligible attenuation coefficient).

$$\begin{bmatrix}\text{Inside}\\ \text{Outside}\end{bmatrix} \frac{\partial^2}{\partial r} + \frac{1}{r}\frac{\partial}{\partial r} + \frac{1}{r}\frac{\partial^2}{\partial \theta^2}\ \psi + \begin{Bmatrix}\mu_1\varepsilon_1\frac{\omega^2}{C^2} - k^2\\ \mu_2\varepsilon_2\frac{\omega^2}{C^2} - k^2\end{Bmatrix}\psi = 0 \qquad (12)$$

The solutions to (12) involve Bessel and Hankel (modified Bessel) functions. As a simple example, ignoring the azimuthal variation, (12) takes the form of Bessel's equation for which the solutions inside and outside the dielectric rod core are given by

$$\psi = \begin{cases} J_0(Ur/a) & r \leq a \\ K_0(Wr/a) & r \geq a \end{cases} \qquad (13)$$

Equation (13) describes the transverse field distributions for the TE_{00} and TM_{00} waveguide modes.

REFERENCES

Collin, R.E. Field Theory of Guided Waves. New York: McGraw-Hill, 1960, p. 484.

Fowles, G.R. Introduction to Modern Optics. New York: Holt, Rinehart and Winston, 1968, p. 49-53.

Imai, M., and Hara, E. "Excitation of Fundamental and Low-order Modes of Optical Fiber Waveguides by Gaussian Beams." Applied Optics 13 (1973):1893-9.

Jenkins, F.A., and White, H.E. Fundamentals of Optics. New York: McGraw-Hill, 1957, p.144.

Marcuse, D. "Excitation of the Dominant Mode of a Round Fiber by a Gaussian Beam." Bell System Technical Journal 49 (1970): 1695-703.

_____. Light Transmission Optics. New York: Van Nostrand Reinhold, 1972, pp. 230-262.

Miller, S.E.; Marcatilli, E.A.J.; and Li, T. "The Transmission Medium." In Optical Fiber Technology, Part I, pp. 5-27. Ed. by D. Gloge. New York: IEEE Press, 1976.

Olver, W.J. "Bessel Functions of Integer Order." In Handbook of Mathematical Functions, 6th ed., pp. 355-433. Edited by M. Abramowitz and I.A. Stegun. Washington, D.C.: U.S. Goverment Printing Office, 1967.

Smith, W.J. Modern Optical Engineering. New York: McGraw-Hill, 1966, pp. 398-405.

Snyder, A.W. "Asymptotic Expressions for the Eigenfunctions and Eigenvalues of a Dielectric or Optical Waveguide." IEEE Transactions on Microwave Theory and Technique MTT-17 (1969): 1130-38.

_____. "Excitation and Scattering of Modes on a Dielectric or Optical Fiber." IEEE Transactions on Microwave Theory and Technique MTT-17 (1969): 1138-44.

Stern, J.R.; and Dyott, R.B. "Off-axis Launching into a Fiber-optical Waveguide." Electronics Letters 7 (1971): 52-3.

Stern, J.R.; Peace, M.; and Dyott, R.B. "Launching into Optical-fiber Waveguide." Electronics Letters 6 (1970): 160-2.

Yariv, A. Introduction to Optical Electronics. New York: Holt, Rinehart and Winston, 1971, p. 30-49.

BIBLIOGRAPHY

Biernson, G., and Kinsley, D.J. "Generalized Plots of Mode Patterns in a Cylindrical Dielectric Waveguide Applied to Retinal Cones." IEEE Transactions on Microwave Theory and Technique MTT-13 (1965): 345-56.

Cardama, A., and Kornhauser, E.T. "Modal Analysis of Coupling Problems in Optical Fibers." IEEE Transactions on Microwave Theory and Technique MTT-23 (1975): 162-9.

Clarricoats, P.J.B. gen. ed. Optical Fiber Waveguides. Hitchin, England: Peter Peregrinus, 1975.

Collin, R.E. Field Theory of Guided Waves. New York: McGraw-Hill, 1960, p. 484.

Fowles, G.R. Introduction to Modern Optics. New York: Holt, Rinehart and Winston, 1968, p. 49-53.

Imai, M., and Hara, E. "Excitation of Fundamental and Low-order Modes of Optical Fiber Waveguides by Gaussian Beams." Applied Optics 13 (1973): 1893-9.

Jackson, J.D. Classical Electrodynamics. New York: John Wiley and Sons, 1962, pp. 259-64.

Jenkins, F.A., and White, H.E. Fundamentals of Optics. New York: McGraw-Hill, 1957, p. 144.

Marcuse, D. "Excitation of the Dominant Mode of a Round Fiber by a Gaussian Beam." Bell System Technical Journal 49 (1970): 1695-703.

_____. Light Transmission Optics. New York: Van Nostrand Reinhold, 1972, p. 230-262.

_____. "Coupled Mode Theory of Round Optical Fibers." Bell System Technical Journal 52 (1973): 817-42.

Miller, S.E.; Marcatilli, E.A.J.; and Li, T. "The Transmission Medium." In Optical Fiber Technology, Part I, pp. 5-27. Ed. by D. Gloge. New York: IEEE Press, 1976.

Olver, W.J. "Bessel Functions of Integer Order." In Handbook of Mathematical Functions, 6th ed., pp. 355-433. Edited by M. Abramowitz and I.A. Stegun. Washington, D.C.: U.S. Government Printing Office, 1967.

Smith, W.J. Modern Optical Engineering. New York: McGraw-Hill, 1966, pp. 398-405.

Snitzer, E. "Cylindrical Dielectric Waveguide Modes." Journal of the Optical Society of America 51 (1961): 491-8.

Snyder, A.W. "Asymptotic Expressions for the Eigenfunctions and Eigenvalues of a Dielectric or Optical Waveguide." IEEE Transactions on Microwave Theory and Technique MTT-17 (1969): 1130-38.

_____. "Excitation and Scattering of Modes on a Dielectric or Optical Fiber." IEEE Transactions on Microwave Theory and Technique MTT-17 (1969): 1138-44.

Stern, J.R.; and Dyott, R.B. "Off-axis Launching into a Fiber-optical Waveguide." Electronics Letters 7 (1971): 52-3.

Stern, J.R.; Peace, M.; and Dyott, R.B. "Launching into Optical-fiber Waveguide." Electronics Letters 6 (1970): 160-2.

Yariv, A. Introduction to Optical Electronics. New York: Holt, Rinehart and Winston, 1971, p. 30-49.